OXYGEN INCORPORATION DURING
LOW-TEMPERATURE CHEMICAL VAPOR DEPOSITION AND
ITS EFFECTS ON THE ELECTRONIC PROPERTIES OF
EPITAXIAL
Si AND $Si_{1-x}Ge_x$ FILMS

Peter V. Schwartz

A DISSERTATION
PRESENTED TO THE FACULTY
OF PRINCETON UNIVERSITY
IN CANDIDACY FOR THE DEGREE
OF DOCTOR OF PHILOSOPHY

RECOMMENDED FOR ACCEPTANCE
BY THE DEPARTMENT OF
ELECTRICAL ENGINEERING

October 1992

Abstract

We describe the status of oxygen in epitaxial silicon and silicon-germanium layers grown by low-temperature chemical vapor deposition. The motivation for this study stems from the drive to increase device and circuit performance by improving the electronic material in which the devices are fabricated. Low-temperature epitaxy provides a method for growing thin epitaxial layers with abrupt interfaces. It can be used with silicon technology to grow $Si/Si_{1-x}Ge_x$ heterojunctions to improve device performance.

The obstacles associated with low-temperature CVD epitaxial growth techniques are rooted in the stability of oxygen on the silicon surface. We demonstrate that oxygen concentrations far above the peak solid solubility can incorporate in epitaxial silicon and silicon-germanium layers grown at low-temperatures. These high concentrations of oxygen are shown to reduce minority carrier lifetimes in heterojunction bipolar transistors, p-n junction diodes, and MOS capacitors. The short carrier lifetimes associated with oxygen contamination of silicon-germanium alloys also reduces the non-radiative recombination lifetimes of the carriers in the $Si_{1-x}Ge_x$ layers so that photoluminescence processes are masked.

We also show that hydrogen passivation of the silicon surface can reduce the probability that oxygen will stick to the growing interface and that the boundary layer can reduce the transport of oxygen to the growth interface, therefore reducing the amount of

oxygen incorporating into the growing film. This is a critical advantage of CVD over MBE, and makes CVD possible with oxygen and water partial pressures far in excess of what is predicted by classical surface science studies. We proceed to show that high-lifetime, low oxygen concentration epitaxial films can be grown at low-temperature in a non-UHV environment, and that improved device performance results.

We then exploit the electronic properties of oxygen doped silicon films for use as semi-insulating epitaxial layers. We demonstrate the crystalline and semi-insulating nature of these films and show that we can grow high-quality silicon films with low oxygen concentrations on top of the oxygen doped layers. This structure provides many opportunities for improved device performance such as MOS transistors and high speed photoconductors.

Acknowledgments

I wish to express my sincere appreciation to the countless people who have helped me during my graduate career.

I am indebted to Dr. James C. Sturm for giving me guidance and a constant stream of ideas over the past five years. His incredible work ethic is an inspiration to me and has served as an excellent model of leadership by example. I feel privileged to have been a member of his research team.

I am grateful to my colleagues in the Sturm group for providing a research atmosphere in which ideas were freely shared, discussed and realized. I am especially grateful to Xiaodong Xiao who was never too busy to answer questions and provide a clear understanding of the problem at hand. His patience when answering the same questions, repeatedly, was greatly appreciated. I have enjoyed friendships I have shared with my colleagues in the Sturm group, especially Erwin Prinz, V. Venkataraman, Zeljka Matutinovic-Krstelj, Chee-Wee Liu, Qun Mi, Casper Reaves and Dr. Peter Garone.

I am indebted to Dr. Lyon and Dr. Prucnal for reading this work and making helpful comments.

Finally, special thanks are due to my wife, Jeannine, for her invaluable support during the past five years. This degree is as much hers as it is mine.

Table of Contents

Chapter 1

Low-Temperature Epitaxy

1.1 Introduction

The drive for improved device performance for high speed integrated circuits is pushing the limits of silicon technology. High speed technology has relied on shrinking lateral device dimensions to minimize the distance electrons must travel within individual devices as well as between devices. Lateral dimensions of state-of-the-art devices have moved into the sub-half micron regime using sophisticated lithographic techniques [1] and are soon to be in production. Device performance has also been improved by utilizing vertical carrier transport in epitaxially grown semiconductor layers. Features on the order of ten nanometers are readily achieved in vertical devices by controlling interface characteristics. Other improvements that are available in vertical devices are gained by heterojunction capabilities. By using the discontinuous band gap between the two semiconductors at the heterojunction, new devices can be engineered to improve device performance. To achieve abrupt interfaces and heterojunctions in silicon technology, low

temperature epitaxy must be employed to minimize dopant inter-diffusion between layers. Low temperature epitaxy is also required for the growth of strained layer alloys needed for heterojunction formation with silicon. This thesis addresses the effect of trace amounts of oxygen gas on low-temperature epitaxial chemical vapor deposition of silicon and silicon-germanium

1.2   Heterojunctions

Heterojunctions offer improved device performance through the formation of a discontinuous band gap at semiconductor interfaces. The discontinuity in the band gap provides a means of engineering new devices for high speed applications such as high mobility field effect transistors [2, 3], heterojunction bipolar transistors [4, 5], and quantum devices (resonant tunneling diodes) [6, 7]. Silicon offers a mature processing technology in VLSI manufacturing and excellent electronic characteristics. However, device and circuit performance can still be improved by the addition of heterojunction capabilities.

Heterojunction performance has, until recently, been reserved for compound semiconductors, and the heterojunction system exploited most is the GaAs - AlAs system. The advantage of this system is that the lattice constants of the two materials differ by less than 0.1%. By varying the concentration of aluminum in $Al_{1-x}Ga_xAs$, the band gap of the material can be continuously tuned from 1.4 eV to 2.2 eV (GaAs to AlAs), with little lattice mismatch. Lattice matching is important for epitaxial growth to avoid the formation of defects at the heterojunction interface.

Unlike III-V semiconductor systems, the silicon system lacks a compatible lattice-matched, band gap-mismatched semiconductor with which a heterojunction can be formed. Gallium phosphide (GaP) is a common semiconductor which has the same lattice constant as silicon, but it is not compatible with silicon technology. Complications arise during the growth of compound semiconductors on silicon substrates because of anti-phase boundary formation caused by steps on the silicon surface [8, 9]. Germanium is the only

semiconductor with properties which show promise of compatibility with silicon technology.

Germanium and silicon form a miscible alloy at every compositional mixture [10]. Since silicon-germanium is a random alloy and not a compound semiconductor, anti-phase boundaries are not an issue during growth. Consequently, the band gap of the silicon can be tuned from 1.12 eV to 0.67 eV (pure silicon to pure germanium) with the addition of germanium [10]. The addition of germanium to silicon changes the intrinsic lattice constant of the material from 5.43 Å to 5.66 Å over the entire range of germanium fraction. If the system retains its intrinsic lattice constant, a lattice-matched epitaxial layer is not formed with silicon. Rather, a defective interface between the materials results. Silicon-germanium alloys can, however, be lattice-matched to silicon if grown under strained conditions. By growing strained layers of silicon-germanium alloys ($Si_{1-x}Ge_x$), defect free, lattice-matched heterojunctions can be formed in a silicon-based material system [11, 12]. For the epitaxial growth of such layers, there are several fundamental and technological reasons which make low temperature growth advantageous. They will be reviewed in the next few sections.

1.3 Strained Layers

Strained-layer growth is depicted in Figure 1.1 with a semiconductor of large lattice constant being grown on a substrate of small lattice constant. Strained-layer growth is needed for defect free epitaxial layers in lattice-mismatched systems. An alloy of 25% germanium ($Si_{0.75}Ge_{0.25}$) will result in roughly a 1% mismatch between the alloy and the silicon substrate. (Germanium has a lattice constant four percent larger than silicon.) Under strained conditions, the lattice constant of the alloy will be compressed in the plane of the wafer to match the substrate and expand in the growth direction according to the Poisson ratio (a material-dependent parameter) for the alloy film. The amount of expansion corresponds roughly to a 0.7% increase in the vertical lattice constant for every 1% mismatch in the horizontal lattice constant [13]. Because of the compression of chemical

3
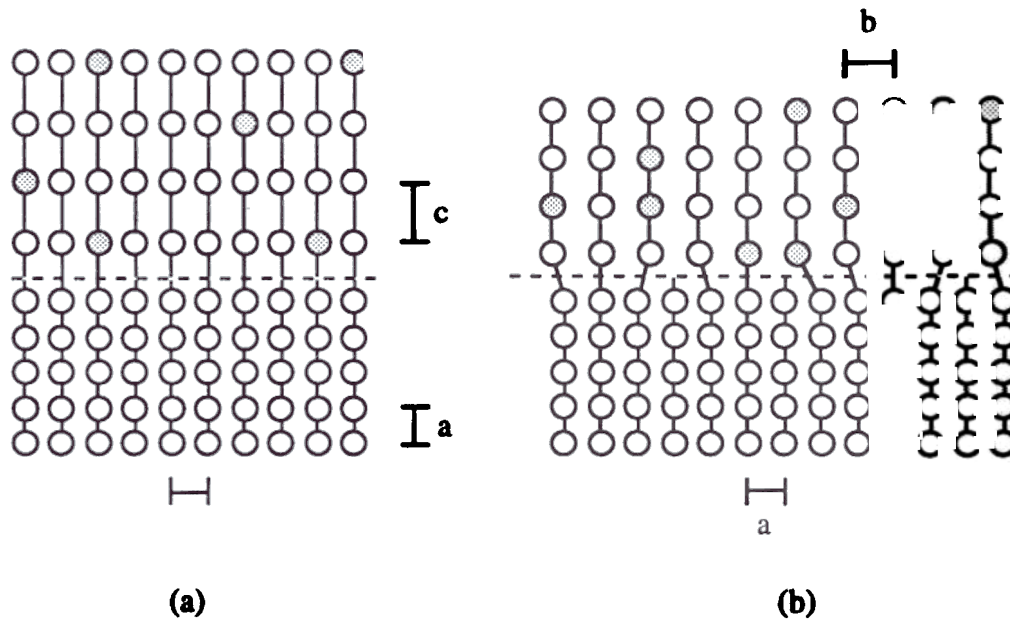
Figure 1.1. Schematic of lattice mismatched growth of a large lattice constant material ($Si_{1-x}Ge_x$) on a small lattice constant material (Silicon). (a) Strained layer epitaxy. The lattice constant of the epitaxial layer is compressed in the horizontal plane to match the lattice constant of the substrate while being elongated in the vertical (growth) direction. (b) Relaxed layer growth. Misfit dislocations run perpendicular to the plane of the paper and serve to relax the layer to a lattice constant different from the substrate. This represents a completely relaxed layer of silicon-germanium on a silicon substrate.

bonds in the alloy, a tremendous amount of energy is stored in these layers. As the energy builds with the growing layer, a competition arises between the energy stored in the bonds and the energy of formation of a misfit dislocation. The energy can be released from the bonds if the formation of a misfit dislocation will lower the total energy of the layer. The thickness of the film at this crossover energy is noted as the critical thickness of strained layer growth and it depends upon the amount of lattice mismatch and hence the germanium concentration in the layer.

A relaxed alloy film due to the formation of misfit dislocations is depicted in Figure 1.1(b). Periodically at the hetero-interface, a plane of atoms appears free of bonds to the epitaxial layer. This extra plane of atoms is a misfit dislocation. A misfit dislocation is a defect in the crystalline material which may be a site for carrier generation or recombination [14] - unwanted sites in minority carrier devices.

The formation of a misfit does not occur immediately when the critical thickness is exceeded. Rather, misfit formation is an energy-activated process (≥ 2 eV) and is therefore highly temperature-dependent [15, 16]. The critical thickness of the film can be greatly exceeded if the temperature of the process is kept to a minimum allowing the growth of metastable strained films. A plot of the critical thickness of $Si_{1-x}Ge_x$ strained to the silicon lattice constant as a function of germanium fraction in the alloy is shown in Figure 1.2. This is a plot based on the theoretical work of Matthews and Blakeslee [17] (1974) and all theory is referenced to their work. The consequences of the equilibrium theory are easily seen by considering a $Si_{1-x}Ge_x$ film of a single germanium concentration with $x = 0.25$.

According to the theory of Matthews and Blakeslee [17], a film containing 25% Ge will have a critical thickness (t_c) of ~100 Å. An alloy layer of this composition, lattice-matched to silicon, grown thinner than t_c will remain strained since it is energetically stable (*i.e.* there is not enough energy stored in the bonds to form a dislocation). A layer grown beyond t_c, which is allowed to find its lowest energy state, will relax to a lattice constant greater than silicon by the formation of misfit dislocations. Films grown beyond t_c can
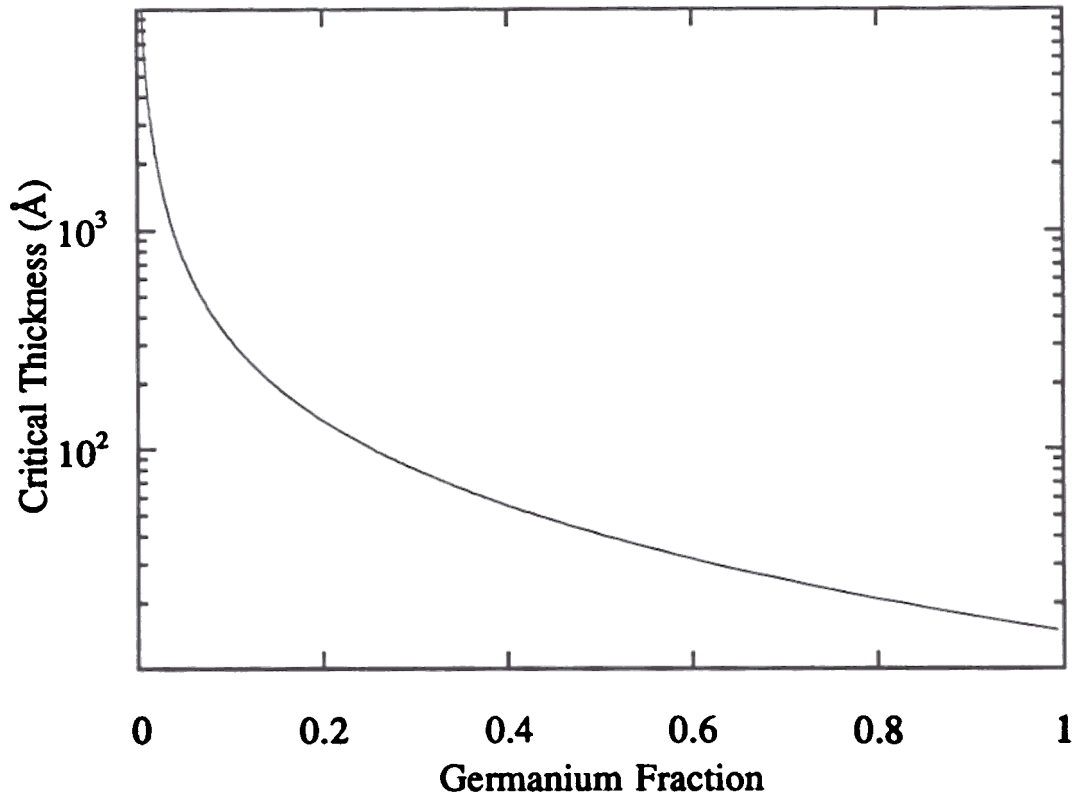
Figure 1.2. Equilibrium critical thickness of silicon-germanium strained to the silicon lattice as a function of germanium concentration in the film. The plot delineates between two regimes: below the line, there is not enough energy stored in the bonds to form a misfit dislocation; above the line, there is enough energy stored in the strained bonds to allow for a misfit dislocation to propagate allowing the layer to relax.

remain strained as long as sufficient energy (in the form of heat , for example) is not provided to drive the system to relaxation. These layers are referred to as "metastable". The fabrication of some devices calls for the deposition of strained layers thicker than that allowed by equilibrium theory. This need for thick, metastable strained layers is one reason for moving to low temperatures for epitaxial growth. By reducing the temperature of strained-layer growth, the excess energy added to the system is minimized, and defect formation avoided.

1.4 Three-dimensional growth

Low temperatures are also required to suppress three-dimensional growth of $Si_{1-x}Ge_x$ layers [18, 19]. Three-dimensional growth is characterized by island formation on the wafer surface (at the growing interface) and leads to non-abrupt junctions between epitaxial layers, as is depicted in Figure 1.3 The Volmer-Weber regime is depicted in Figure 1.3(b) and is seen as island formation directly on the substrate and is typical of silicon growth on germanium. The Stranski-Kranstanov is shown in Figure 1.3(c) where layer-by-layer (two dimension growth) occurs initially before islands form on the growing surface. This regime is typical of germanium growth on silicon. Both of these growth regimes lead to a roughened growth front. One way to suppress these regimes of growth and achieve layer-by-layer (Franck-Van der Merwe) growth is to lower the growth temperature [19] and reduce surface migration to prevent island formation. For example, for $Si_{0.85}Ge_{0.15}$ layers on silicon, we have found that at 750 °C hazy surfaces result even below critical thickness. This was avoided by reducing the growth temperature below 700 °C where specular reflection from the surfaces was achieved, indicating two-dimensional growth

1.5 Layer thickness control

1.5.1 Solid state diffusion

Low-temperature growth is also advantageous for minimizing dopant diffusion as well as increasing layer thickness control. At low temperatures, silicon epitaxial growth by
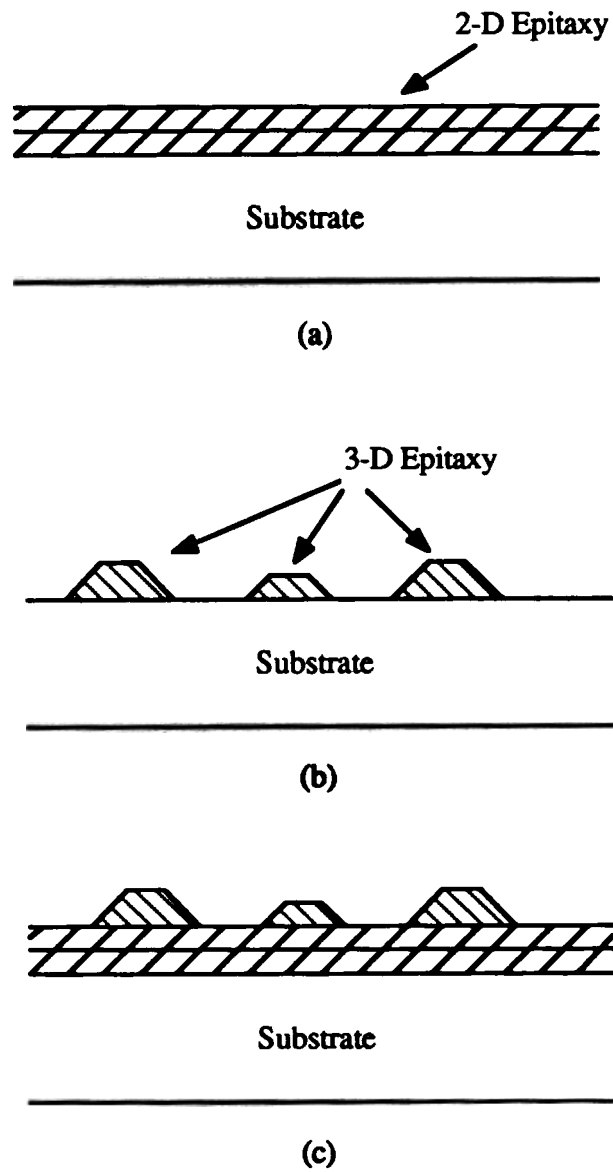
Figure 1.3. Two-dimensional growth *vs.* three dimensional growth. (a) Two-dimensional growth which is desired for uniform layer thickness. (b) Three-dimensional growth. Volmer-Weber regime where islands form directly on the substrate. (c) Stranski-Kranstanov regime where islands form after a few layers of two-dimensional growth.

chemical vapor deposition is dominated by surface chemical reactions and is therefore strongly temperature dependent with an activation energy around 2 eV [19]. Dopant diffusion is also an energy-activated process strongly dependent upon temperature, with an activation energy around 3.5 eV (Ref. [20] tabulates the activation energies of several of the common impurities in silicon). Figure 1.4 is a plot of the growth rate of a silicon film as a function of inverse temperature. The rate of boron diffusion is also plotted on the same temperature scale. Because the activation energy of dopant diffusion is higher than that of the growth rate, the rate of dopant diffusion decreases faster with temperature than does the growth rate of the silicon film. Note that most dopants (phosphorous and arsenic) have similar activation energies to boron. By growing films at low temperatures, we can stack alternating layers of doped and undoped material while retaining well-defined interfaces because the diffusion of dopants from the doped layers into the undoped layers is minimized.

1.5.2   Reduced growth rates

Figure 1.4 also illustrates the added control over layer thickness that is a consequence of growth at reduced temperatures. At low temperatures, the growth rate is dominated by surface reactions which can be very slow (surface reaction limited regime), while at high temperatures (>850 °C), the growth rate is fairly insensitive to temperature and is determined by how quickly the gases hit the substrate surface (mass transport limited regime) [14]. Growing structures with layer thicknesses of 100 Å is more precise at a growth rate of 50 Å/min (~ 700 °C) than at 2500 Å/min (~ 1000 °C). At 1000 °C, a one second time differential translates into a 50% error in thickness whereas at 700 °C a one second time differential corresponds to a 1% error in film thickness. Clearly, for small device dimensions, a reduced growth rate is preferable.

All of the reasons given above point in the direction of low temperature growth of epitaxial layers: hetero-epitaxial growth, interface abruptness, reduced dopant diffusion, and layer thickness control. Low temperature growth of silicon and silicon-germanium,
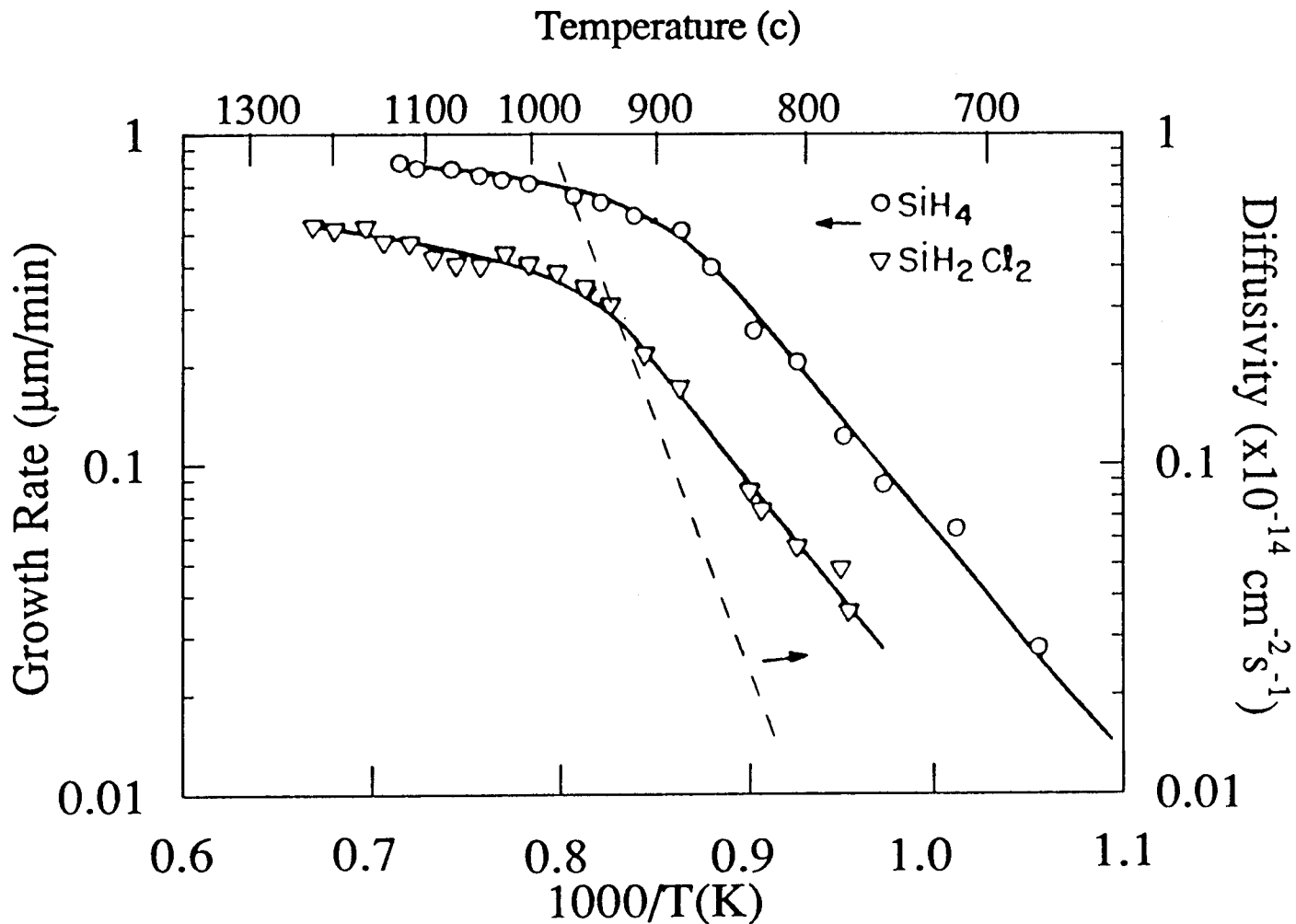
Figure 1.4. Growth rate and Boron diffusion rate as a function of temperature. The activation energy for the growth rate data is ~ 2 eV while the activation energy for boron diffusion is ~ 3.5 eV (most dopants have similar activation energies). This implies that the diffusion rate of dopants decreases more quickly with temperature than does the growth rate of the film. Therefore, alternating layers of doped material and undoped material can be grown with sharp interfaces. After Ref. [19].

however, is not without its problems. The problems related to low temperature epitaxy of silicon and silicon-germanium are centered around the increased stability of oxygen on the surface of silicon substrates, that is, at the growing interface.

1.6 Problems with low-temperature epitaxy

Epitaxial growth requires a clean substrate upon which to grow. If oxygen is in the environment, this can lead to SiO_2 formation on the substrate surface. The formation of SiO_2 during epitaxial growth is due to trace contaminants of oxygen or water in the gas sources or from outgassing of the reactor components. Precipitates of SiO_2 create highly defective crystals which lead to poly-crystalline layers [21]. Oxygen also readily incorporates into the growing film at low temperature leading to oxygen levels far above the peak solid solubility [22, 23]. The effect of these high concentrations of oxygen on the electronic properties of the film will be discussed in detail in Chapter 5. In general, oxygen is a lifetime-limiting contaminant in silicon. The standard solution to the problem of oxygen contamination during growth has been to perform epitaxial growth at temperatures above 800 °C. Above this temperature, oxygen readily desorbs from the silicon surface in the form of SiO leaving behind an oxygen-free, crystalline surface on which to grow [24,25,26]. Typical industrial procedures use temperatures in excess 1000 °C to avoid these problems. However, we have already seen that this temperature range is not conducive to hetero-epitaxy or thin layer epitaxy.

There are several techniques for growing epitaxial silicon, and the two most common low-temperature techniques are molecular beam epitaxy (MBE) and chemical vapor deposition (CVD). We choose to study silicon and silicon-germanium layers grown by rapid thermal CVD (RTCVD) because CVD is the most common technique used for growing epitaxial silicon films. The technique is easily incorporated into large scale production of integrated circuits since it is a multi-wafer process. Also, ultra-high vacuum (UHV) conditions are not required which keeps equipment costs low and also avoids unnecessary complications to production equipment.

11

The remainder of this work deals with the growth of high-quality silicon and $Si_{1-x}Ge_x$ strained layers by low temperature chemical vapor deposition and the effect of oxygen contamination on the electronic properties of the epitaxial layers. The organization of the thesis is presented below.

1.7 Thesis Structure

Chapter 2 discusses oxygen incorporation during epitaxial growth of silicon and some of the historical reasons for problems with low-temperature CVD. The experimental goal is also defined in this chapter.

In Chapter 3 we discuss the experimental procedures for studying oxygen incorporation in low-temperature CVD growth. We discuss the measurement techniques used to determine the oxygen concentrations in the films and characterize the structural form of the oxygen within the silicon lattice.

We determine the effective sticking coefficient for oxygen during CVD growth in Chapter 4 and we establish the conditions for growing low-oxygen content films at low temperatures. Hydrogen is shown to play a critical, beneficial role during CVD.

We discuss the effects of oxygen on the electronic properties of the films in Chapter 5. We report minority carrier generation and recombination lifetimes of low oxygen content films and contrast them to oxygen-doped films.

In Chapter 6, we propose a novel material based on oxygen-doped silicon films for fabricating electronic devices. We discuss the semi-insulating nature of oxygen-doped silicon and its uses for forming semi-insulating substrates in silicon.

We conclude with Chapter 7 and a summary and discussion of the directions of future work.

1.8 References

1   K. Nakagawa, M. Taguchi and T. Ema, "Fabrication of 64M DRAM with i-Line Phase-Shift Lithography," *Tech. Dig. IEDM 90* (33.1.1) (1990).

2. M. Abe, T. Mimura, N. Kobayashi, M. Suzuki, M. Kosugi, M. Nakayama, K. Odani and I. Hanyu, "Recent Advances in Ultra-high Speed HEMT LSI Technology," *IEEE Trans. Elec. Dev.* , **TED-36** (10), 2021 (1989).

3. D.K. Nayak, J.C.S. Woo, J.S. Park, K.-L. Wang and K.P. MacWilliams, "Enhancement-Mode Quantum-Well Ge_xSi_{1-x} PMOS," *IEEE Elect. Dev. Lett.* **EDL-12**(4), 154 (1991).

4. P.M. Asbeck, M.-C. F. Chang, J.A. Higgins, N.H. Sheng, G.J. Sullivan and K.-C. Wang, "GaAlAs/GaAs Heterojunction Bipolar Transistors: Issues and Prospects for Application," *IEEE Trans. Elec. Dev.* **TED-36**(10), 2032 (1989).

5. S.S. Iyer, G.L. Patton, J.M.C. Stork, B.S. Meyerson and D.L. Harame, "Heterojunction Bipolar Transistors Using Si-Ge Alloys," *IEEE Trans. Elec. Dev.* **TED-36**(10), 2043 (1989).

6   F. Capasso, K. Mohammed and A.Y. Choi, "Resonant Tunneling Through Double Barriers, Perpendicular Quantum Transport Phenomena in Superlattices, and Their Device Applications," *IEEE J. Quant. Elec.* **QE-22**(9), 1853 (1986).

7. H.C. Liu, D. Landheer, M. Buchanan and D.C. Houghton, "Resonant Tunneling in $Si/Si_{1-x}Ge_x$ Double Barrier Stuctures," *Appl. Phys. Lett.* **52**(21), 1809 (1988).

8   S. Wright, H. Kroemer and M. Inada, "Molecular Beam Epitaxial Growth of GaP on Si," *J. Appl. Phys.* **55**(8), 2916 (1984).

9. W.I. Wang, "Molecular Beam Epitaxial Growth and Materials Properties of GaAs and AlGaAs on Si (100)," *Appl. Phys. Lett.* **44**(12), 1149 (1984).

10. R. Braunstein, A.R. Moore and F. Herman, "Intrinsic Optical Absorption in Germanium-Silicon Alloys," *Phys. Rev.* **109**(3), 695 (1958).

11. E.A. Fitzgerald, Y.-H. Xie, D. Brasen, M.L. Green, J. Michel, P.E. Freeland and B.E. Weir, "Elimination of Dislocations in Heteroepitaxial MBE and RTCVD Ge_xSi_{1-x} Grown on Patterned Substrates," *J. Elect. Mater.* **19**(9), 949 (1990).

12. D.A. Grutzmacher, T.O. Sedgwick, A. Zaslavski, R.A. Kiehl, A.R. Powell and I.M. Fisher, " Growth of SiGe/Si Quantum Well Structures by Atmospheric Pressure Chemical Vapor Deposition," *Elect. Mat. Conf.*, Boston (1992).

13. U. Schmid, N.E. Christensen, M. Alouani and M. Cardona, "Electronic and Optical Properties of Strained Ge/Si Superlattices," *Phys. Rev.* B**43**(18), 43 (1991).

14. K.V. Ravi, "Imperfections and Impurities in Semiconductor Silicon," Wiley, New York (1981).

15. R. Hull and J.C. Bean, "Thermal Stability of $Si/Ge_xSi_{1-x}/Si$ Heterostructures," *Appl. Phys. Lett.* **55**(18), 1900 (1989).

16. R. Hull, J.C. Bean, D. Noble, J. Hoyt and J. F. Gibbons, "Dependence of Misfit Dislocation Velocities Upon Growth Technique and Oxygen Content in Strained $Ge_xSi_{1-x}/Si(100)$ Heterostructures," *Appl. Phys. Lett.* **59**(13), 1585 (1991).

17. J.W. Matthews and A.E. Blakeslee, "Defects in Epitaxial Multilayer Structures - I: Misfit Dislocations," *J. Cryst. Growth* **27**, 118 (1974).

18. D.J. Eaglesham and M.Cerullo, "Low-temperture Growth of Ge on Si(100)," *Appl. Phys. Lett.* **58**(20), 2276 (1991).

19. F.C. Eversteyn, "Chemical Reaction Engineering In The Semiconductor Industry," *Philips Res. Rept.* **19**, 45 (1974).

20. S. Wolf and R.N. Tauber, "Silicon Processing for the VLSI era: Volume I," Lattice Press, Sunset Beach, CA (1986).

21. K.V. Ravi, "Imperfections and Impurities in Semiconductor Silicon," Wiley, New York (1981).

22. M.L. Green, D. Brasen, M. Geva, W. Reents, Jr., F. Stevie and H. Tempkin, "Oxygen and Carbon Incorporation in Low Temperature Epitaxial Si Films Grown by Rapid Thermal Chemical Vapor Deposition (RTCVD)," *J. Elec. Mater.* **19**(10), 1015 (1990).

23. P.V. Schwartz, J.C. Sturm, P.M. Garone and S.A. Schwarz, "Extreme Supersaturation of Oxygen in Low Temperature Epitaxial Silicon and Silicon-Germanium Alloys," *Proc. Mat. Res. Soc.* **163**, 591 (1989).

24. G. Ghidini and F.W. Smith, "Interaction of H_2O with Si (111) and (100)," *J. Electrochem. Soc.* **31**(12), 2924 (1984).

25. F.W. Smith and G. Ghidini, "Reaction of Oxygen with Si(111) and (100): Critical Conditions for the Growth of SiO_2," *J. Electrochem. Soc.* **129**(6), 1300 (1982).

26. J.J. Lander and J. Morrison, "Low Voltage Electron Diffraction Study of the Oxidation and Reduction of Silicon," *J. Appl. Phys.* **33**(6), 2089 (1962).

Chapter 2

The Role of Oxygen in Silicon Technology

2.1 Oxygen in Silicon

The study of oxygen in silicon emerged in the middle 1950's with the infrared absorption work of Kaiser, Keck and Lange [1]. They extended the knowledge of the Si-O bond in quartz to determine the nature of the 1107 cm^{-1} (~9 μm) absorption peak in silicon. They determined the relationship between the strength of this absorption (absorption coefficient) and the total interstitial oxygen concentration in the film. Many important characteristics of silicon grown by the Czychrolski (Cz) pull method were then determined from this relationship. Kaiser *et al.* determined the peak solid solubility of interstitial oxygen in the silicon lattice (~2 x 10^{18} cm^{-3}) [2] and the effects of reactor ambient on the oxygen incorporation during float zone refining of silicon crystals [1]. Kaiser *et al.* also [2] investigated the variation of oxygen content with vertical position in the silicon ingot

and the radial distribution of oxygen in the silicon ingot. After these early works, interest in oxygen in silicon waned in the 1960's until the boom of the silicon VLSI era around 1970.

In the 1970's studies of the production yields in semiconductor manufacturing found that the wafers cut from the seed end of the Cz-silicon ingot had a significantly higher product yield than those cut from the tail portion of the ingot. Without a clear understanding as to the cause, there was little chance to control the production yield. With this finding, the interest in the properties of oxygen in silicon was rekindled. It had been determined many years earlier (by Kaiser *et al.* [2]) that the oxygen concentration in the seed end of the ingot was much higher than that of the tail portion in Cz silicon because of the interaction between the silicon melt and the quartz crucible used to hold the charge. The oxygen (at levels $\leq 10^{18}$ cm^{-3}) was found to be beneficial because oxygen precipitates added mechanical strength to silicon particularly during high temperature processing [3, 4] and because of the ability of the precipitates to getter unwanted metal impurities [5, 6]. The importance of oxygen in silicon technology was then shown to extend far beyond the formation of insulating layers of silicon dioxide. All of these studies, however, concern oxygen concentration levels at or below the peak solid solubility of oxygen in silicon (~ 2 x 10^{18} cm^{-3}).

Because of the importance of SiO_2 in the semiconductor industry, the study of oxygen and its interaction with the silicon surface has also been studied extensively. Numerous works related to the initial stages of oxide growth have investigated the stability of oxygen on the surface of silicon (Ref. [7] contains an extensive reference listing of the major work in this area.) Surface scientists have concentrated on the initial formation of chemical bonds and the stability of oxygen on clean silicon surfaces at reduced [8] and elevated temperatures [9, 10, 11].

The stability of oxygen on a silicon surface at elevated temperatures has great implications in the low temperature growth of crystalline silicon. For chemical vapor

deposition (or any crystalline growth technique), a clean defect-free surface is needed for crystalline growth. Precipitates, which can arise from oxide formation, break the pattern of the silicon substrate and cause non-crystalline growth and highly defective films which result in the formation of stacking faults and hillock structures [12, 13]. It is the stability of oxygen on the silicon surface which is of concern during CVD growth since oxygen tends to play a detrimental role in terms of crystalline quality and crystal purity.

2.2 Stability of Oxygen on Silicon

Experimental results of Lander and Morrison (1962) [9] and later by Ghidini and Smith (1983) [10, 11] have been used as a guideline by which epitaxial reactor designers determine operating points. Figure 2.1, from the Lander and Morrison study, describes the stability of oxygen on the clean surface of silicon in the temperature range of 600 °C to 1000 °C and an oxygen pressure of 7×10^{-9} Torr to 10^{-4} Torr. (The work of Ghidini and Smith extended the temperature of the Lander experiment to 1300 °C and included a study of the stability of water on a silicon surface.) Lander and Morrison described the competing processes of adsorption and desorption of oxygen on silicon by the formation of SiO_2 with the following equations: [9]

$$\frac{1}{2} O_{2(g)} \rightarrow O_{(ads)} \qquad\qquad [2.1]$$

$$Si + 2O_{(ads)} \rightarrow SiO_2 \qquad\qquad [2.2].$$

They describe desorption of oxygen in the form of silicon monoxide by:

$$Si + SiO_2 \rightarrow 2SiO_{(g)}. \qquad\qquad [2.3]$$

We discuss the experimental set up used in the UHV measurements of Lander *et al.* and Ghidini *et al.* for contrast to the conditions used during CVD growth. Lander *et al.* and Ghidini *et al.* used slightly different experimental techniques, however their experimental results were consistent. The stability experiments were carried out in an ultra-high vacuum chamber with a base pressure of $< 10^{-9}$ Torr and with a clean silicon substrate. The substrates were heated to ~1300 °C for five minutes to clean the surface of oxygen and then the temperature was lowered to the desired operating point. Oxygen was then carefully
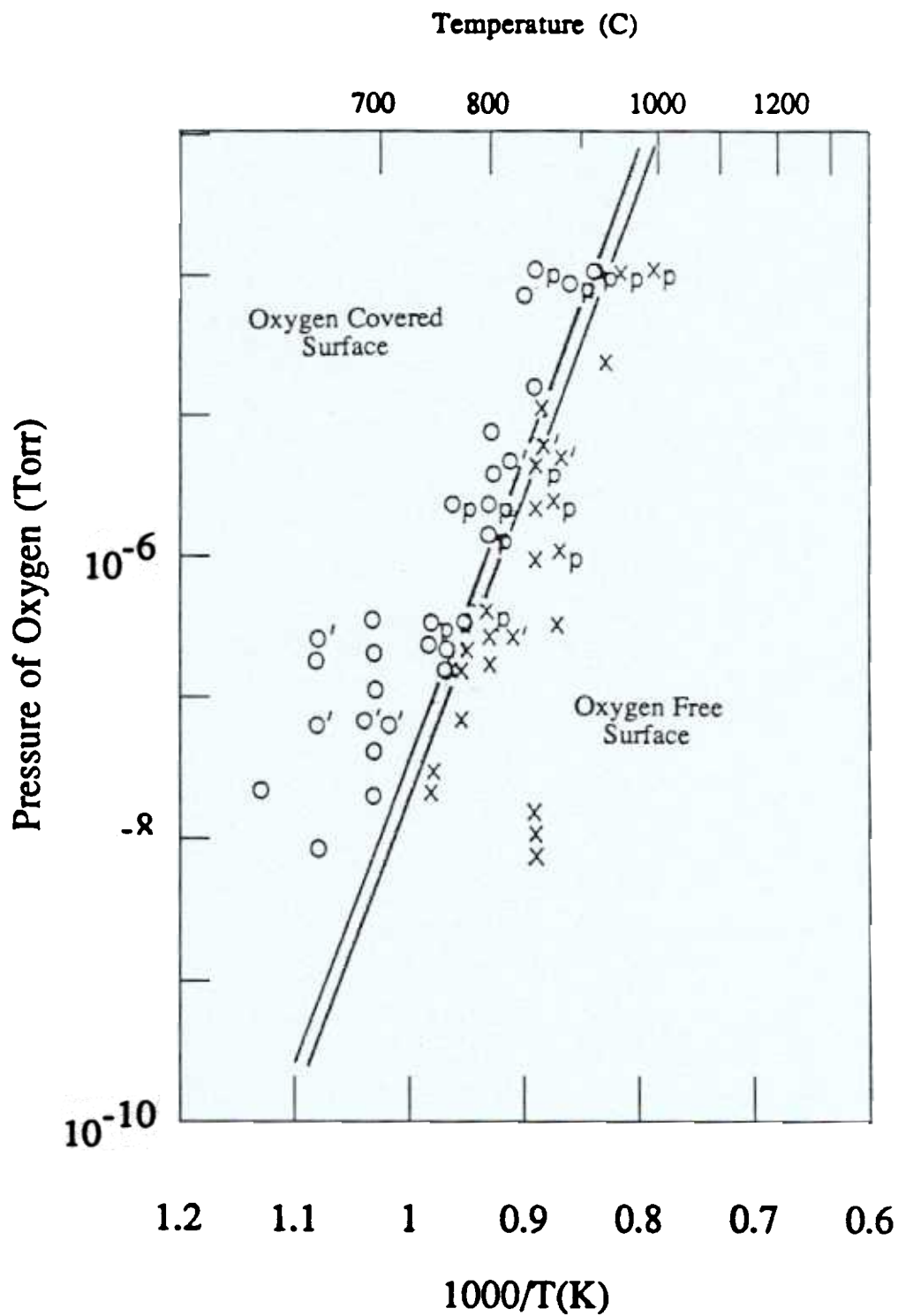
18

Figure 2.1. Oxygen stability on the surface of silicon. This is the data of Lander and Morrison showing the stability of oxygen on the clean surface of silicon. The line in the plot delineates conditions of oxide-covered and oxide-free surfaces. As one moves to high temperatures and low pressures of oxygen, the surface remains clean. Ref.[10].

19

introduced to the reactor to a specified partial pressure for the experiment. At each temperature the system was allowed to establish a steady state condition before measurements were made. The stability of oxygen was determined by LEED patterns in the Lander experiment. Under the conditions of oxygen contamination (oxide formation), the symmetry of the LEED pattern is broken making it easy to determine the crossover from an oxide-free (clean) to an oxide-covered surface. The measurement technique was sufficiently sensitive to determine surface coverage down to a few percent of one monolayer. Ghidini and Smith measured the emissivity change of the substrate from an oxide free condition to an oxide covered condition to determine the critical crossover.

According to both studies, as the partial pressure of oxygen in the chamber increases and the substrate temperature decreases, oxygen remains more stable on the substrate surface forming SiO_2 because the desorption rate depends exponentially on temperature (Figure 2.1). The sticking probability of molecular oxygen on the clean surface was found to be approximately 0.01 and relatively independent of temperature and in good agreement with the experimental data of Hagstrum [14], who had previously performed measurements on oxygen adsorption (1961). Ghidini and Smith found a similar trend for the temperature and pressure dependencies of the interaction of water vapor with the clean silicon surface [10]. Under the conditions of high substrate temperature and low oxygen pressure, the surface remains free of oxygen due to the desorption of SiO leaving behind the crystalline pattern of the substrate. The line in Figure 2.1 delineates the regimes of an oxide covered surface and an oxide-free surface. It is this line which has determined historically the conditions for epitaxial growth; we will show this to be overly pessimistic.

2.3 Oxygen Contamination During CVD

The results of Lander and Morrison indicate that in order to obtain an oxygen free silicon surface at 700 °C, the partial pressure of oxygen in the reactor atmosphere must be below 10^{-8} Torr. Consequently, for a growth pressure of one atmosphere, the source

20

gases must be purified to a level below 0.01 parts O_2 per billion (ppb) parts source gas. This is beyond the range of gas purifiers available today (gas purifiers can guarantee ~ 10 ppb O_2) [15]. Similar arguments can be made for water vapor, (which in practice may be worse than O_2), but we will give arguments and experiments for O_2 throughout this thesis, keeping in mind the principles will relate to H_2O as well. We chose to study O_2 in these experiments instead of H_2O because O_2 does not stick to the walls of the reactor and the partial pressure of oxygen in the reactor decreases quickly as the gas flow is turned off. These aspects are important so that we do not introduce contaminants into subsequent experiments.

To circumvent the restriction on gas purity, Meyerson at IBM developed the technique of UHV-CVD [16]. By reducing the growth pressure to 10^{-3} Torr as done in UHV-CVD, Meyerson relaxed the condition of gas purity by several orders of magnitude. With a growth pressure of 10^{-3} Torr, the source gas purity need only be 10,000 ppb to remain below the 10^{-8} Torr of oxygen required for a clean silicon surface at 700 °C. Requiring UHV conditions on CVD growth are rather extreme and the central point of this thesis is that one does not need to move to ultrahigh vacuum conditions for CVD growth. As proof, we demonstrated that high quality oxygen-free silicon films could be grown in a non-UHV system at 700 °C and 6 Torr by CVD [17] and soon after, Sedgwick and Agnello [18] (also at IBM) demonstrated high quality epitaxial silicon at 750 °C in an atmospheric pressure CVD reactor. (Our work and techniques will be discussed in detail in Chapters 3 and 4.) Clearly, the criteria imposed by Lander and Morrison (and Ghidini and Smith) are too pessimistic when dealing with CVD growth conditions. During CVD growth, a steady state condition different from the UHV clean surface situation is established between the oxygen and the silicon. Furthermore, the hydrogen present in CVD would be expected to cause a fundamental difference between UHV experiments and CVD growth.

A dynamic surface condition is established on the substrate during CVD growth under which a clean surface in continuously being created as the film grows. As oxygen sticks to the surface it is constantly being buried by the growth of new silicon. The oxygen is trapped in the growing film and not allowed to migrate and form clusters of SiO_2 on the surface because of the low diffusion rate of oxygen at temperatures below 750 °C (~ 8 x 10^{-14} cm^2s^{-1}) [19]. This continuous burying of oxygen allows concentrations of oxygen to incorporate into the silicon at levels far above the peak solid solubility (~ 10^{18} cm^{-3}), without the formation of SiO_2. This allows for the growth of crystalline layers since the pattern of the substrate is not broken by precipitate formation. The fact that we can incorporate levels of oxygen far above the solid solubility means that oxygen incorporation is governed by a kinetic process rather than an equilibrium process during low temperature growth. Incorporation levels above the solid solubility have also been observed for boron doping of low-temperature epitaxial films [20] without precipitation and is attributed to a kinetic burying process at low temperatures as opposed to an equilibrium process.

A second argument why the conditions on gas source contamination can be relaxed during CVD growth concerns the reactor ambient. CVD is performed typically in a hydrogen ambient and hydrogen is also abundant in the source gases. This leads to a hydrogen passivated surface at temperatures above the hydrogen desorption temperature of 550 °C. As silane decomposes on the surface of the wafer, the silicon bonds which extend up from the substrate are terminated by hydrogen atoms [21]. The surface of the silicon will tend to remain hydrogen covered since the reactor ambient is almost entirely H_2. The plausibility of this argument is supported by simple thermodynamic principles stated below.

The study of hydrogen passivation and its effect on the CVD growth temperature has been investigated by several researchers [22, 23], yet little work has been done to investigate the hydrogen passivation of silicon with a hydrogen over-pressure as actually occurs during CVD. The H_2 interaction with the silicon surface has been studied

sufficiently, however, to determine some chemical equilibrium rate constants. The Si (100) surface is terminated by single hydrogen atoms, yet desorption takes place as a hydrogen molecule:

$$H_{2(g)} \iff 2H_{(a)} \qquad\qquad [2.4]$$

where the equilibrium rate constant is given as $K_{eq} = k_a/k_d$ (k_a and k_d are the adsorption and desorption rates respectively) and is related to the Gibb's free energy of the reaction by K_{eq} = exp (-$\Delta G/kT$). Since $\Delta G = \Delta H$ - TΔS, where H is the enthalpy of the reaction (~2 eV) [24] and S is the entropy (~4 eV/K) [25], a value for K_{eq} can be approximated. The fraction of surface coverage (θ_H) as a function of hydrogen gas pressure (P_{H2}) is found from K_{eq} as: [26]

$$\theta_H = \frac{K_{eq} \cdot P_{H2}}{1 + K_{eq} \cdot P_{H2}} \qquad\qquad [2.5]$$

Figure 2.2 shows the approximate value for hydrogen surface coverage (θ_H) as a function of temperature under our standard growth conditions of 6 Torr H_2. For example, although the hydrogen desorption temperature is 550 °C (in UHV temperature programmed desorption studies), the surface remains ~ 99.8% covered at 700 °C. This hydrogen termination effectively reduces the sticking coefficient of oxygen on silicon by tying up available sites. This is shown schematically in Figure 2.3. Under these high coverage conditions, the oxygen sticking probability does not go to zero since oxygen is allowed to physisorb to the surface and migrate before it finds either an open site (chemisorbs) or is removed by the gas stream. The physisorption of molecules on surfaces is the consensus explanation for the invariance of sticking coefficient with surface coverage (up to 80% - 90% surface coverage [27]) and the breakdown of the Langmuir models [26] for surface adsorption. The dependence of the sticking coefficient is still debated (some researchers claim Langmuir adsorption ∝ coverage^{-1}). However, it is clear that the sticking probability is reduced under conditions of high surface coverage. Since the silicon surface is hydrogen terminated, the probability that the adsorbed oxygen sites are dense enough to form clusters
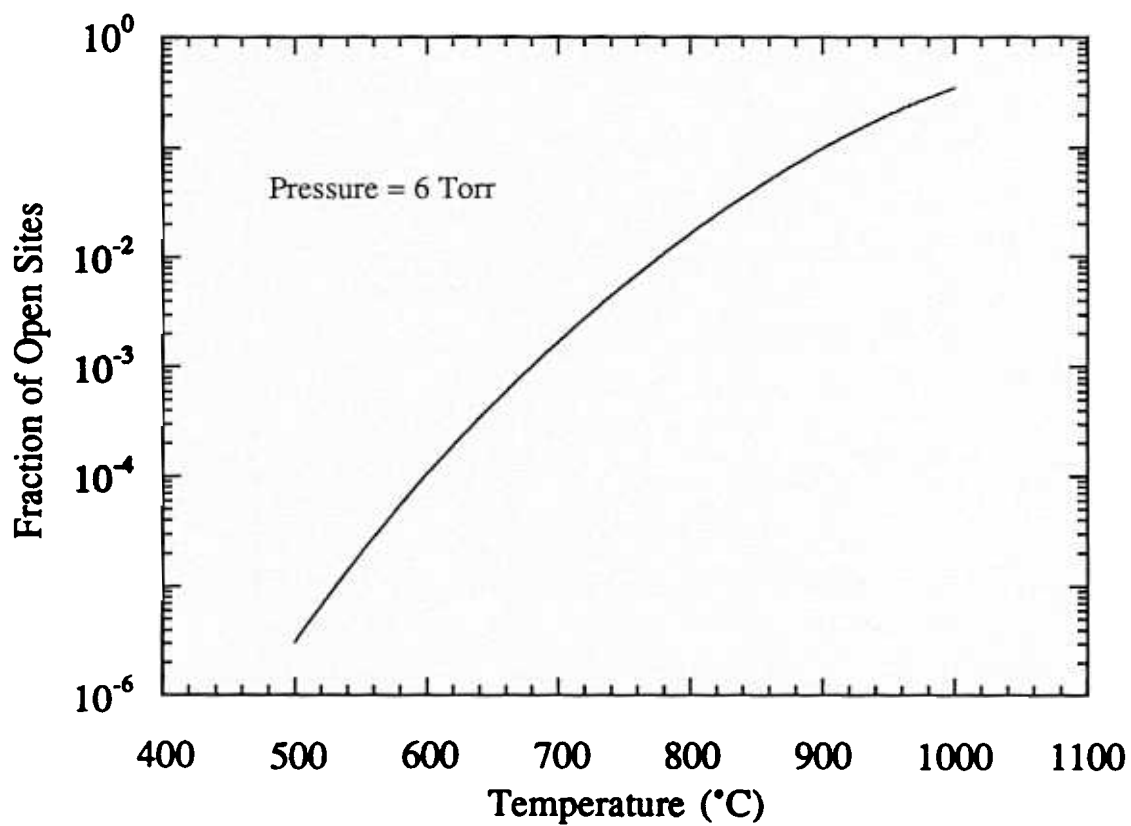
Figure 2.2. Hydrogen surface coverage as a function of substrate temperature for a hydrogen pressure of 6 Torr. Notice at 700 °C, the silicon surface is still 99.8 % covered with hydrogen.

24
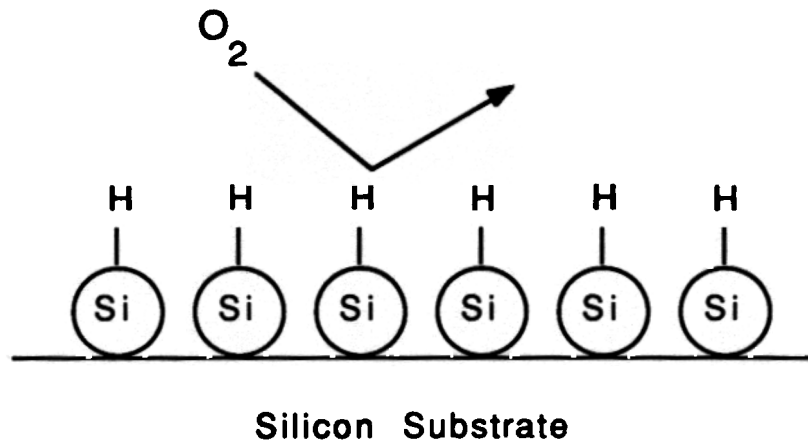
Figure 2.3. Hydrogen passivated surface. Most of the silicon surface is covered with hydrogen so an impinging oxygen molecule sees an almost completely covered surface and is prevented from sticking to the surface. The surface remains hydrogen terminated even at 700 °C because of the hydrogen over-pressure in the system.

before being buried is lowered and the effective sticking coefficient of oxygen on silicon is also reduced.

A third factor which determines the effective sticking of oxygen on a silicon surface during CVD growth is the formation of a boundary layer in a viscous flow regime. A semi-stagnant layer is established above the growth substrate due to the frictional drag of gas across the wafer surface. Since gas molecules must diffuse vertically across this boundary layer in order to interact with the growing surface, many of the gas molecules pass through the system without seeing the growth surface. This boundary layer, in effect, cuts down the amount of oxygen molecules which strike the wafer surface. We shall see in the following chapters that the presence of the boundary layer and the hydrogen passivation of the surface both play an important role in reducing the amount of oxygen which incorporates into the growing film.

Our purpose in this study is to determine the conditions for growth of clean silicon and silicon-germanium epitaxial layers by chemical vapor deposition at low temperature (< 800 °C). To determine the conditions for growing high quality films, we must study the characteristics of oxygen incorporation in the epitaxial films during growth and determine the effective sticking coefficient of oxygen. Once the effective sticking coefficient is measured, we can proceed to determine the conditions for growing low oxygen content films and we will show that this can be done without UHV conditions. We can then contrast the electronic properties of the films doped with oxygen and those which are oxygen free and show that the presence of large amounts of oxygen (> 10^{19} cm^{-3}) in the low temperature epitaxial layers reduces the minority carrier lifetimes in the films, and has detrimental effects on minority carrier devices.

26

2.4 References

1. W. Kaiser, P.H. Keck and C.F. Lange, "Infrared Absorption and Oxygen in Silicon and Germanium," *Phys. Rev.* **101**(4), 1264 (1956).

2. W. Kaiser and P.H. Keck, "Oxygen Content of Silicon Single Crystals," *J. Appl. Phys.* **28**(8), 882 (1957).

3. S.M. Hu and W.J. Patrick, "Effects of Oxygen on Dislocation Movement in Silicon," *J. Appl. Phys.* **46**(5), 1869 (1975).

4 S.M Hu, "Dislocation Pinning Effect of Oxygen Atoms in Silicon," *Appl. Phys. Lett.* **31**(2), 53 (1977).

5. G.A. Rozgonyi, R.P. Deysher and C.W. Pearce, "The Identification, Annihilation, and Suppression of Nucleation Sites Responsible for Silicon Epitaxial Stacking Faults," *J. Electrochem. Soc.* **123**, 1910, (1976).

6. G.H. Schwuttke, " Study of Copper Precipitation Behavior in Silicon Single Crystals," *J. Electrochem. Soc.* **108**, 163 (1961).

7. M.P. D'Evelyn, M.M. Nelson and T. Engel, " Kinetics of the Adsorption of O_2 and the Desorption of SiO on Si(100): A Molecular Beam, XPS, and ISS Study," *Surf. Sci.* **186**, 75 (1987).

8 A.J. Schell-Sorokin and J.E. Demuth, "Low Temperature Oxidation of Silicon (111) 7 x 7 Surfaces," *Surf. Sci.* **157**, 273 (1985).

9 J.J. Lander and J. Morrison, "Low Voltage Electron Diffraction Study of the Oxidation and Reduction of Silicon," *J. Appl. Phys.* **33**(6), 2089 (1062).

10. G. Ghidini and F.W. Smith, "Interaction of H_2O with Si (111) and (100)," *J Electrochem. Soc.* **31**(12), 2924 (1984).

11. F.W. Smith and G. Ghidini, "Reaction of Oxygen with Si(111) and (100): Critical Conditions for the Growth of SiO_2," *J. Electrochem. Soc.* **129**(6), 1300 (1982).

12. K.V. Ravi, Imperfections and Impurities in Semiconductor Silicon, Wiley, New York (1981).

13. R.H. Finch, H.J. Queisser, G. Thomas and J. Washburn, "Structure and Origin of Stacking Faults in Epitaxial Silicon," *J. Appl. Phys.* 34(2), 406 (1963).

14 H. Hagstrum, "Oxygen Adsorption on Silicon and Germanium," *J. Appl. Phys.* 32(6), 1020 (1961).

15. Operation Manual, Nanochem® Gas Purifier, Semi-gas Systems, Inc., San Jose (1988).

16. B.S. Meyerson, "Low-temperature Silicon Epitaxy by Ultrahigh Vacuum/Chemical Vapor Deposition," *Appl. Phys. Lett.* 48(12), 797 (1986).

17. P.V. Schwartz, J.C. Sturm and C. Magee, "Reduction of Oxygen Incorporation and Lifetime Measurements in Epitaxial $Si_{1-x}Ge_x$ Films Grown by Low Temperature Rapid Thermal CVD," *Elect. Mat. Conf.* Santa Barabara, CA (1990).

18. T.O. Sedgwick, M. Berkenbilt and T.S. Kuan, " Low-temperature Selective Epitaxial Growth of Silicon at Atmospheric Pressure," *Appl. Phys. Lett.* 54(26), 2689 (1989).

19. J.C. Mikkelsen, Jr., "Diffusivity of Oxygen in Silicon During Steam Oxidation," *Appl. Phys. Lett.* 40(4), 336 (1982).

20. B.S. Meyerson, F.K. LeGoues, T.N. Nguyen, and D.L. Harame, "Nonequilibrium Boron Doping Effects in Low-temperature Silicon Films," *Appl. Phys. Lett.* 50(2), 1987.

21. M. Liehr, *Appl. Phys. Lett.* 56, 629 (1990).

22. S.H. Wolff, S. Wagner, J.C. Bean, R.Hull and J.M. Gibson, " Hydrogen Surface Coverage: Raising the Epitaxial Growth Temperature," *Appl. Phys. Lett.* 55(19).

23. M. Copel and R.M. Tromp, " Are Bare Surfaces Detrimental in Epitaxial Growth?" *Appl. Phys. Lett.* 58(23), 2648 (1991).

24. K. Sinniah, M.G. Sherman, L.B. Lewis, W.H. Weinberg, J.T. Yates, Jr.and K.C. Janda, "New Mechanism for Hydrogen Desorption from Covalent Surfaces: the Monohydride Phase on Si(100)," *Phys. Rev. Lett.* **62**(5), 567 (1989).

25. J. Benzinger, *private communication.*

26. M.A. Morris, M. Bowker and D.A. King, "Kinetics of Adsorption, Desorption and Diffusion at Metal Surfaces," Comprehensive Chemical Kinetics **19**, Elsevier, Amsterdam (1984).

27. P.E. Wierenga, A. Van Silfhout and M.J Sparnaay, "Reflection Study of Dangling-bond Surface States and Oxygen Adsorption on the Clean Si(111) 7 x 7 Surface," *Surf. Sci.* **87**, 43 (1979).

Chapter 3

Experimental Procedures and Techniques

3.1 Introduction

In this chapter we describe the experimental apparatus and procedures used in the study of oxygen incorporation and the material characterization of the heavily doped oxygen layers grown by RTCVD. We start with a description of the Rapid Thermal Chemical Vapor Deposition system and highlight a few of its key features. Included in this chapter is a brief discussion of temperature measurement because of its importance in low temperature CVD growth. We describe a measurement technique we developed to overcome inherent temperature measurement problems. The experimental procedure for introducing oxygen into the epitaxial films and measurement techniques used to characterize the oxygen concentrations and structural properties of these films are then presented. The data analysis will be presented in the next chapter.

3.2 Experimental Apparatus

The Rapid Thermal Chemical Vapor Deposition (RTCVD) reactor used in our experiments is shown in Figure 3.1. The Princeton RTCVD reactor is a non-UHV system consisting of a quartz reaction tube, cooled by forced nitrogen, surrounded by a gold-plated reflector assembly. The reflector assembly houses a bank of twelve high-intensity (6 kW) tungsten-halogen lamps which are used to externally heat the silicon substrate. The lamp radiation passes through the quartz chamber with minimum absorption to heat the silicon substrate which rests on a quartz stand inside the reaction chamber; there is no graphite susceptor used in this system.

The source gases are: silane (SiH_4) and dichlorosilane (DCS - $SiCl_2H_2$) for silicon, germane (GeH_4) for germanium, and phosphine (PH_3) and diborane (B_2H_6) as n and p type dopants, respectively. These gases are introduced into the reaction chamber in a hydrogen carrier through a series of calibrated mass flow controllers and the system is exhausted by a rotary vane pump. The pressure of the system is measured with a capacitance manometer and is controlled by a throttle valve on the exhaust line which alters the pumping speed. The system is equipped with a turbo-molecular pump for low pressure epitaxial growth and for achieving base pressure. To date, all epitaxial growth in our reactor has been performed around 10 Torr using only the mechanical pump.

The system also utilizes a load-lock for sample loading and unloading. The loading chamber on the reactor prevents atmosphere from contaminating the system between each deposition. Water vapor and oxygen, which adsorb to the quartz wall and subsequently desorb during growth, becoming incorporated in the growing film, are kept from entering the reaction chamber in this way. The use of the load-lock allows us to maintain the system at low pressure at all times and minimize background contamination.

The base pressure of the reactor is approximately 10^{-8} Torr and is determined by pumping the unit overnight with the turbo-molecular pump and measuring with pressure with an ion gauge. The leak rate of the reactor is $\sim 10^{-6}$ Torr l s^{-1}. Operating the system at
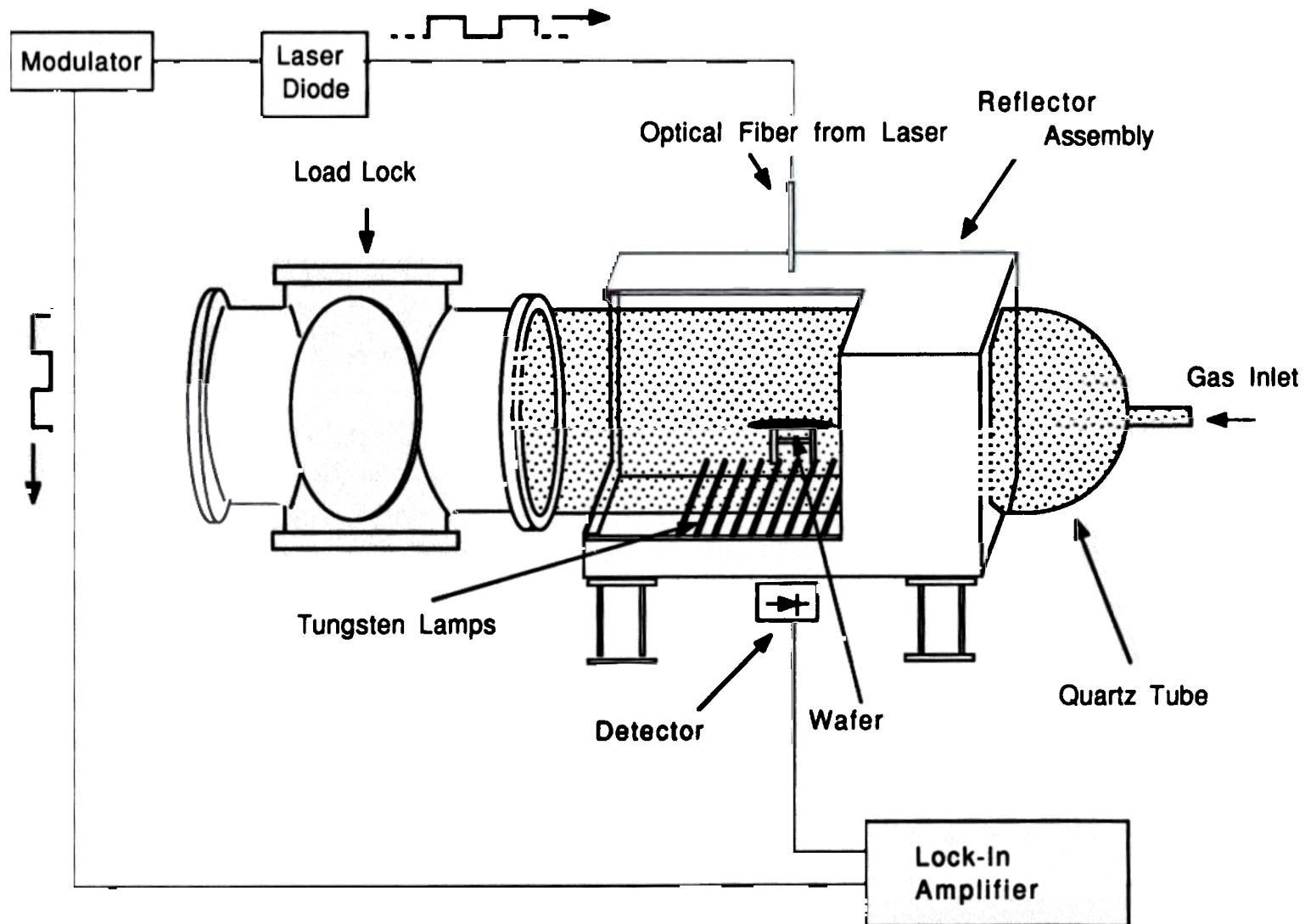
31

Figure 3.1. Schematic drawing of the Princeton RTCVD reactor. Key features are labled on the figure.

10 Torr in a hydrogen carrier means that the oxygen contamination level due to the reactor background is less than 1 ppb. Assuming an infinitely pure source gas, this fulfills the requirement imposed by Lander and Morrison in the previous chapter for maintaining an oxide free surface at 700 °C. As will be seen in Chapter 4, this is an overly sensitive view for CVD.

The small thermal mass of the wafer allows the temperature to be increased at a rate of 200 °C/sec in our reactor which proves useful when growing alternating layers at different temperatures. Since the primary use of rapid thermal systems is for high temperature anneals of short duration ($\geq$ 800 °C for 30 seconds) [1] to minimize dopant diffusion, temperature measurement must be fast and accurate. Some CVD systems utilize this rapid thermal capability to grow epitaxial layers by switching the chemical reaction of growth on and off with the substrate temperature (a process called Limited Reaction Processing [2]). We choose to switch the gas flows rapidly during growth instead of rapidly switching temperature. The transients involved with gas switching in our reactor are less than 2 seconds which corresponds less than one mono-layer of growth at 700 °C. However, we still need the ability to rapidly switch temperature when growing alternating layers of silicon and strained silicon-germanium (silicon layers are typically grown at 700 °C while the silicon-germanium strained layers are grown at 625 °C). We monitor the temperature of the silicon substrate during growth using a temperature measurement technique designed at Princeton.

3.3 Temperature measurement

Temperature control is extremely important during low temperature (< 800 °C) CVD growth of silicon because the growth rate is exponentially dependent upon temperature [3] (see Figure 1.4). The exponential temperature dependence of growth rate has pronounced effects on dopant concentrations as well as alloy film composition [4, 5, 6]. Absolute temperature control is also important for long term reproducibility of experimental results. These same considerations must be addressed in our oxygen doping

33

experiments in order to obtain an accurate effective sticking coefficient and to ensure that we remain below the SiO desorption temperature of 850 °C.

In lamp-heated, susceptorless systems (rapid thermal systems in general), accurate temperature measurement is difficult since a thermocouple is not easily integrated into the system. Typical optical techniques used to measure temperature such as pyrometry [7] are difficult since they require a knowledge of the emissivity of silicon which is itself strongly temperature dependent [8]. Also, at operating temperatures below 700 °C, the quartz walls of the reactor are opaque to the wavelengths needed for temperature measurement by optical pyrometry (~ 5μm) [9]. To solve the problem of temperature measurement, we developed a technique based on the temperature dependence of the optical transmission of 1.3μm and 1.55 μm light through a silicon wafer [10, 11]

Many properties of silicon are temperature-dependent and are measurable during growth. Two of the largest effects are those of band gap narrowing and increased carrier concentration with increased temperature. At room temperature, silicon is transparent to both 1.3 and 1.55 μm light [12] (see Figure 3.2) but as the temperature of the silicon is increased, the silicon becomes increasingly opaque at these wavelengths due to high free-carrier absorption and valence band to conduction band absorption. As benchmarks, the band gap of silicon at 600 °C is approximately 0.93 eV (1.33 μm), at 700 °C ~ 0.89 eV (1.39 μm) and at 750 °C ~ 0.87 eV (1.42 μm) with intrinsic carrier concentrations of 2 x 10^{17}, 5 x 10^{17}, 8 x 10^{17} cm^{-3}, respectively. Since the absorption edge in silicon is not abrupt with respect to energy, we can measure the increase in temperature of the wafer due to a gradual change in transmission of infrared light. The effect of increasing temperature on the absorption edge of silicon is to shift the curve of Figure 3.2 to the left i.e. to lower energies. Figure 3.3 shows the temperature dependence of the absorption coefficient at 1.3 μm and 1.55 μm in the temperature range of 400 °C to 800 °C.

The increased phonon population [13] (needed for band-to-band carrier generation in the indirect band gap material) and the band gap narrowing with increased temperature
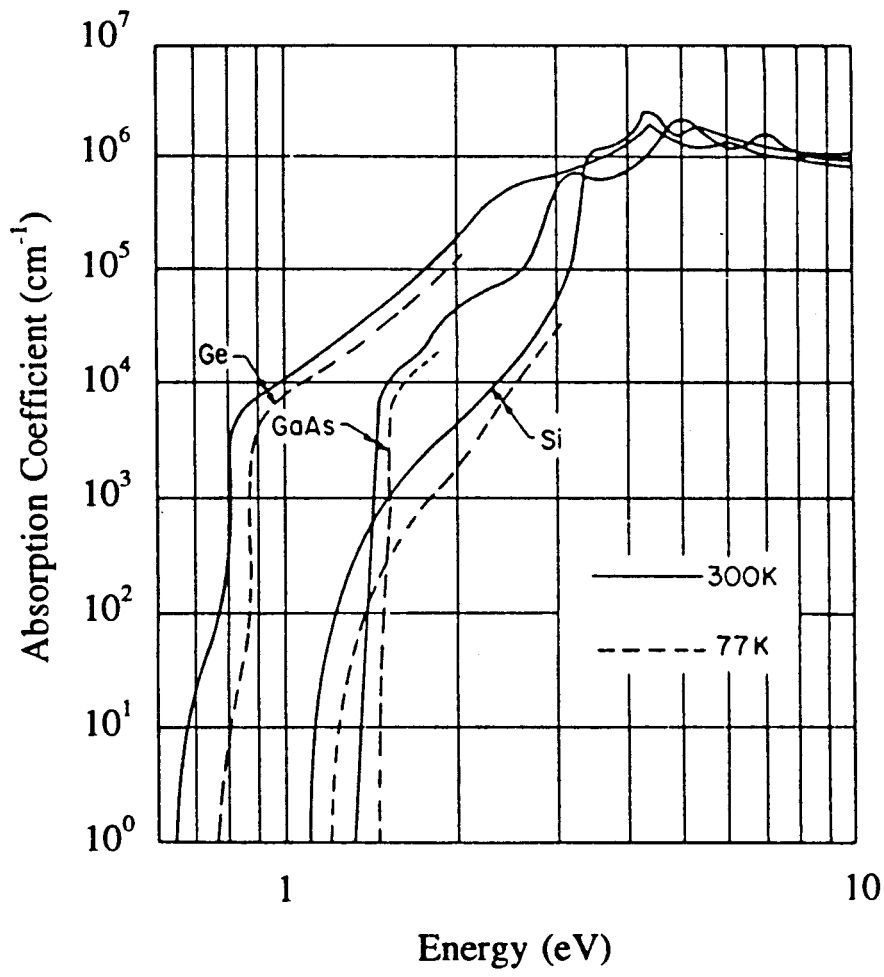
Figure 3.2. Absorption coefficient of Si, Ge, and GaAs (after Sze). The absorption of silicon increases gradually when compared to GaAs. This is due to the indirect nature of the silicon band gap. Heating silicon would move the absorption edge to the left making the material more opaque to longer wavelength light.
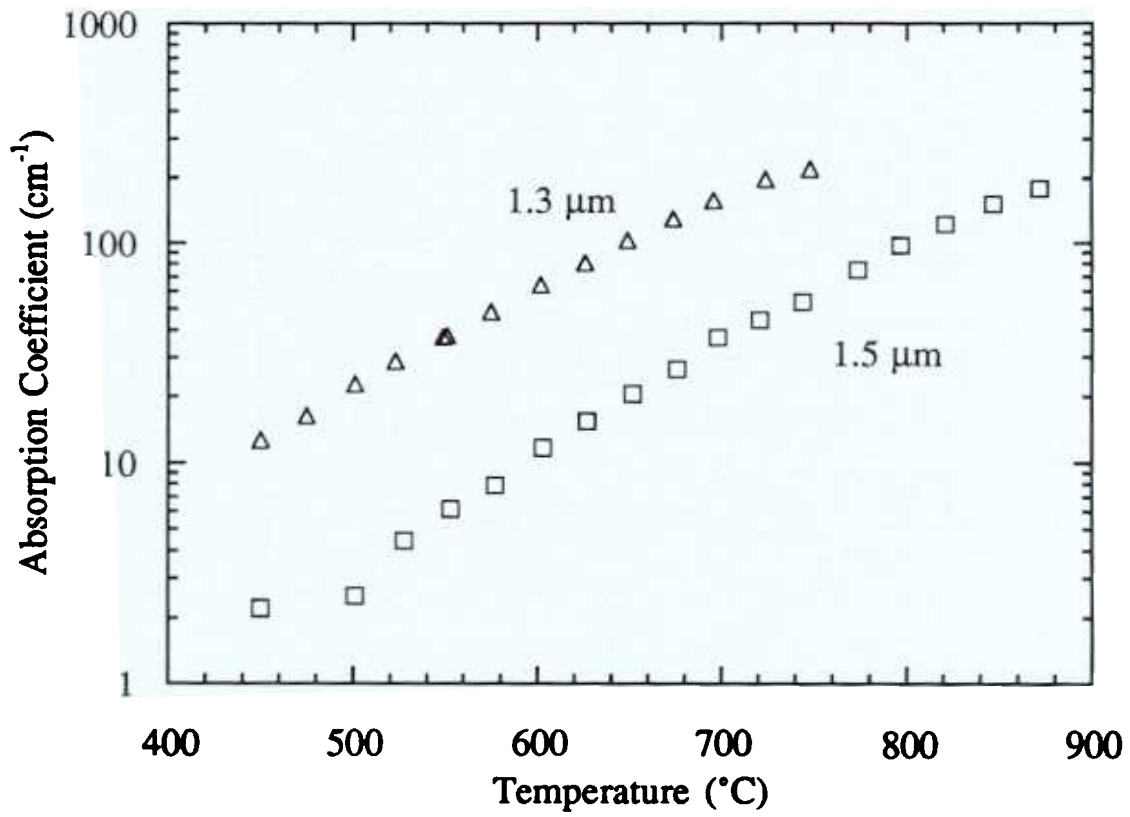
Figure 3.3. Absorption coefficient of silicon between 400 °C and 900 °C for 1.3 μm and 1.5 μm light. Ref. [10].

first push the absorption edge above the 1.3 μm wavelength [14]. The effect is a decrease in 1.3 μm transmission through the wafer with an increase in temperature. The decrease in 1.55 μm transmission comes mainly from increased free carrier absorption in the silicon [14]. As the temperature is further increased, the intrinsic carrier concentration is also increased and the free carrier absorption of the 1.55 μm light is enhanced. The final result is a probe of temperature from 400 °C - 650 °C with the 1.3 μm laser and from 600 °C - 800 °C with the 1.55 μm laser.

The intensity of light transmitted through the substrate depends exponentially upon its thickness according to:

$$I(T,d) = I_0 K (1-R)^2 \exp[-\alpha(T)d] \qquad [3.1]$$

where $I(T,d)$ is the intensity of light transmitted, I_0 is the incident intensity, R is the amount of light reflected from the surface (1-R varies less than 2% over the temperature range of 200 °C - 700 °C), $\alpha(T)$ is the temperature dependent absorption coefficient and d is the wafer thickness. K is a geometrical factor which includes backside surface scattering and light collection efficiency, which is assumed to be a constant of the system for a given wafer. For applications to RTCVD, the transmitted intensity is normalized by the room temperature transmission signal. This normalization eliminates K and $(1-R)^2$ from Eqn. 3.1 which can be expressed as:

$$t(d,T) = \exp(-\alpha \cdot d) \qquad [3.2]$$

where $t(d,T)$ is the normalized transmission ratio. The normalized transmission curve for 1.3 μm and 1.55 μm light shown in Figure 3.4. The absolute temperature scale was determined with a thermocouple welded to the surface of as 440 μm thick silicon substrate. The value used for normalization, during standard growth sequences, is the room temperature transmission signal after 1.5 μm buffer layer growth at 1000 °C.

The transmission data of Figure 3.4 is easily extended to substrates of arbitrary thickness, by examining Eqn. 3.2 and the following relationship:

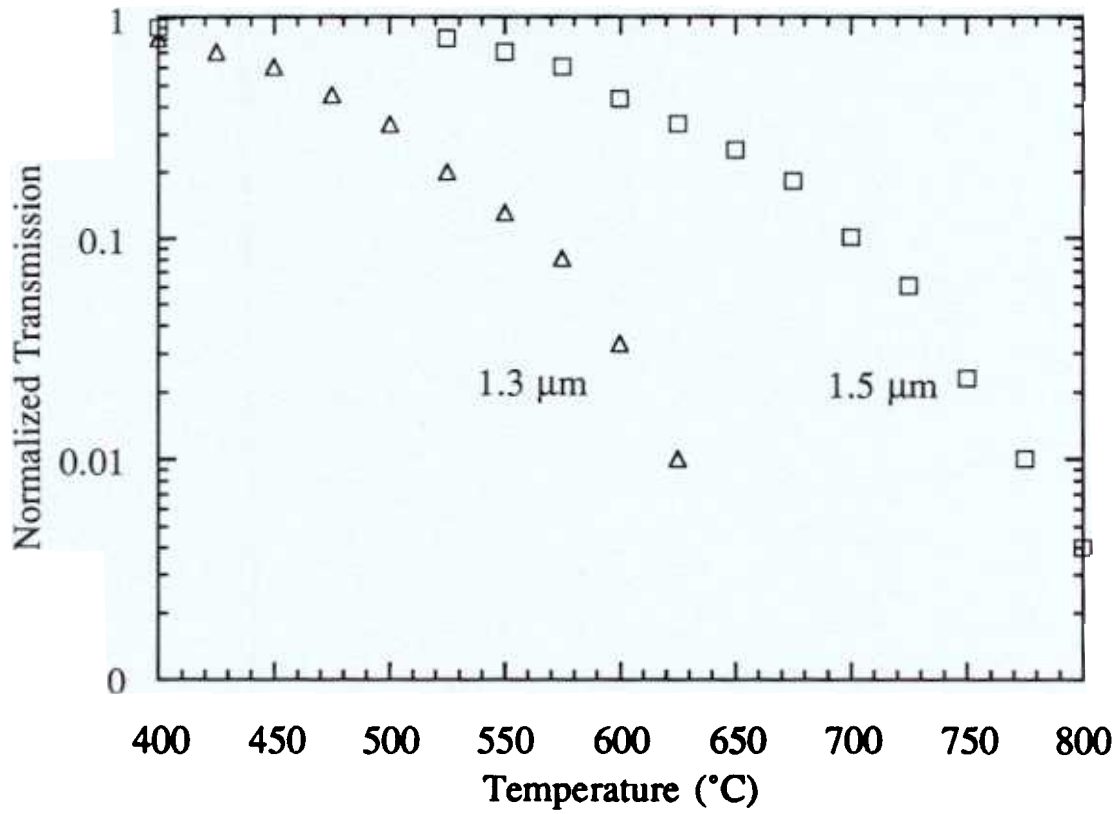$$\log[t(T,d_{sub})] = \frac{d_{sub}}{d_{std}} \log[t(T,d_{std})] \qquad [3.3]$$

Figure 3.4. Normalized transmission data used for determining the substrate temperature during growth. The triangles represent the 1.3 μm laser data. The 1.5 μm data is represented by squares. The wafer thickness is 440 μm. Ref. [10].

where $t(T,d_{sub})$ is the normalized transmission ratio of the test sample substrate at a given temperature, $t(T,d_{std})$ the normalized transmission ratio of the calibration wafer at the same temperature (taken from Figure 3.4) and d_{sub} and d_{std} the sample and calibration substrate thicknesses, respectively. This relationship makes this measurement technique extremely powerful since it can be used on wafers of arbitrary thickness and illustrates the accuracy of this technique for use during epitaxial growth. An error in wafer thickness of 5 μm corresponds to ~ 1 °C temperature error in the range near 600 °C. Since typical layer thicknesses grown are on the order of 1 μm for silicon and less than 1000 Å for strained silicon-germanium the result is a very small error in temperature during growth. Strained layers of $Si_{1-x}Ge_x$ ($\leq$ 1000 Å, $x \leq$ 0.45 Å) and 1.1 μm of unstrained $Si_{0.55}Ge_{0.45}$ were found to have less than a 20% effect on the optical transmission near 1.3 μm and 1.55 μm [15].

The sensitivity of this measurement technique is found from the slope of $t(T)$ in Figure 3.4. For example, at 750 °C, one degree resolution requires detecting a 3% relative change in the 1.55 μm signal which is easily achieved with simple electronics. Near 600 °C, a one degree resolution requires detection of a 4% relative change in the transmitted signal from the 1.3 μm laser. A one degree temperature resolution with the 1.55 μm laser at 600 °C would require detecting less than a 1% change in relative signal. Clearly, for highest resolution, it is advantageous to operate at the shortest wavelength which gives a detectable signal. A detailed procedure for this temperature measurement technique is given elsewhere [16].

3.4 Experimental Procedure

For standard growth sequences, all silicon substrates are cleaned chemically in a bath of H_2O_2:H_2SO_4 (1:1) for a minimum of twenty minutes and then dipped in a HF:H_2O (1:50) solution for 1 minute prior to loading. This leaves the surface terminated with hydrogen and helps to prevent oxygen contamination during loading [17]. The substrates are then placed in a loading chamber which was back-filled three times with nitrogen and

evacuated to 50 mTorr between back-fills before the substrate is passed into the growth chamber

The substrate temperature is ramped to approximately 1000 °C in 40 seconds to undergo a 60 second clean in a hydrogen ambient (250 Torr) to remove any residual oxide from the substrate surface The 1000 °C temperature is not controlled but is approximated from the temperature vs. lamp-power for a wafer with a thermocouple welded to the surface. The reactor pressure is then reduced to 6 Torr for growth. For temperature control purposes, a 1.5μm buffer layer is grown at 1000 °C using dichlorosilane (DCS) as the silicon source in a hydrogen carrier (26 sccm DCS in 3 slpm of H_2). (Buffer layer growth is not performed in all growth sequences, they were, however, for the oxygen experiments.) The wafer is then cooled to room temperature for the temperature normalization with the hydrogen flow maintained during the wafer cooling. The wafer temperature is then ramped to 1000 °C (in 40 sec. in H_2) before the DCS is injected for an additional 0.25 μm buffer layer. The temperature is then lowered to the experimental temperature. No contamination (oxygen, carbon, etc.) is found at the interface formed by the temperature normalization when studied by Secondary Ion Mass Spectrometry (SIMS).

For growth of alternating layers of silicon and silicon-germanium, the DCS and hydrogen are continuously flowing while the temperature is being switched between 625 °C ($Si_{1-x}Ge_x$ growth) and 700 °C (silicon growth) and vice versa. The temperature is allowed to stabilize for ten seconds at 625 °C before the germane is switched on at the beginning of the $Si_{1-x}Ge_x$ layer growth, and the germane is switched off five seconds (to purge the tube of germane) before the temperature is returned to 700 °C for the silicon growth. In the case of oxygen-doped silicon growth, the ten second temperature rule and five second gas purging rule also apply

We introduce controlled amounts of oxygen to the gas flow during low temperature epitaxial growth to determine the incorporation kinetics. The oxygen was introduced with an argon carrier (~ 280 ppm O_2 in Ar) through a calibrated mass flow controller so the

oxygen concentration in the reactor could be regulated. Initial experiments were performed during growth with DCS as the silicon source, but the introduction of oxygen reduced the growth rate of the film and eventually halted the deposition of silicon. One hypothesis to explain this observation is that a layer of oxide forms on the surface of the wafer and we enter a selective growth regime. The HCl present in the DCS cleans the oxidized surface so no silicon is deposited. This is the principle which allows us to grow on silicon islands surrounded by oxide with no deposition on the oxide covered surface[18]. No such growth rate reductions were noticed when silane was used as the source gas, and, the majority of the experiments were therefore performed using silane as a silicon source. We did not pursue the DCS and O_2 further.

For a silane source (~10 sccm), oxygen concentrations in the gas flow ranged from 0.05 ppm to 100 ppm over a growth temperature range of 600 to 850 °C. The oxygen concentrations in the silicon films were determined by Fourier Transform Infrared Spectroscopy (FTIR) and also by Secondary Ion Mass Spectrometry (SIMS). FTIR transmission measurements were used because of the strong absorption of the silicon-oxygen bond and the well characterized relationship between the absorption coefficient and the oxygen concentration in the film [19].

3.5 Infrared Spectroscopy

Fourier Transform Infrared Spectroscopy (FTIR) is a non-invasive technique for determining the presence of certain chemical bonds in a material. It is especially useful for determining the presence of impurity atoms such as oxygen and carbon in crystalline silicon.

Kaiser *et al.* [19] determined the conversion factor between the absorption coefficient (α) and the number of interstitial oxygen atoms (N_0) (at 1107 cm^{-1}) in silicon as 4.9 x 10^{17} cm^{-2} for an absorption band with a full width at half maximum (FWHM) of 32 cm^{-1}. This conversion factor was confirmed by vacuum fusion analysis. The conversion

factor and the FWHM have since become semiconductor standards for measuring the concentration of oxygen in silicon [19].

Figure 3.5 shows typical FTIR spectra of silicon films heavily doped with oxygen (a) - (c) and spectra of interstitial oxygen (d) and silicon containing oxygen precipitates (e). For oxygen concentrations below $10^{20}cm^{-3}$ the films reflect light specularly. Due to the temperature non-uniformity of the substrate surface during growth, we see radial color patterns on the wafer surface. This indicates a film thickness non-uniformity across the wafer as well as an index of refraction difference between the substrate and the epitaxial layer. For oxygen concentrations above $2 \times 10^{20} cm^{-3}$ the edges of the wafer become hazy and reflect light diffusely. We expect the oxygen concentration at the edge of the wafer to be higher than the center due to the reduced substrate temperature and growth rate and hence an increase in defect formation.

In Figure 3.5, the peak absorption of the band shifts to higher energies (higher wavenumber) with increasing oxygen concentration and all of the FWHM are larger than the accepted standard for interstitial oxygen in silicon. The exact coordination of the oxygen in the silicon lattice is not known, however this trend suggests that the oxygen may be entering substitutional sites as well as interstitial sites. The shift of the peaks is the same as the shifts associated with the formations of SiO and $SiO_{1.5}$ [20] seen in oxygen-doped silicon epitaxial films (OXSEF) grown by MBE [21]. Concentrations of oxygen in the OXSEF films reach levels of 30% atomic [22, 22]. The appearance of a peak at 865 cm^{-1} (due to a non-bridging oxygen [23] in heavily doped samples (Fig. 3.5(c)) suggests that the oxygen is introducing defects in the form of non-bridging oxygen. However, no poly-silicon peaks are visible in the X-ray diffraction spectrum.

The broadening of the absorption may be caused by both the phase mixing of the silicon and oxygen as well as by the strain induced in the system. Raman spectra of our oxygen doped films show a broadening of the silicon line characteristic of strain [24]. Low temperature FTIR measurements may shed light on the coordination of the oxygen atoms.
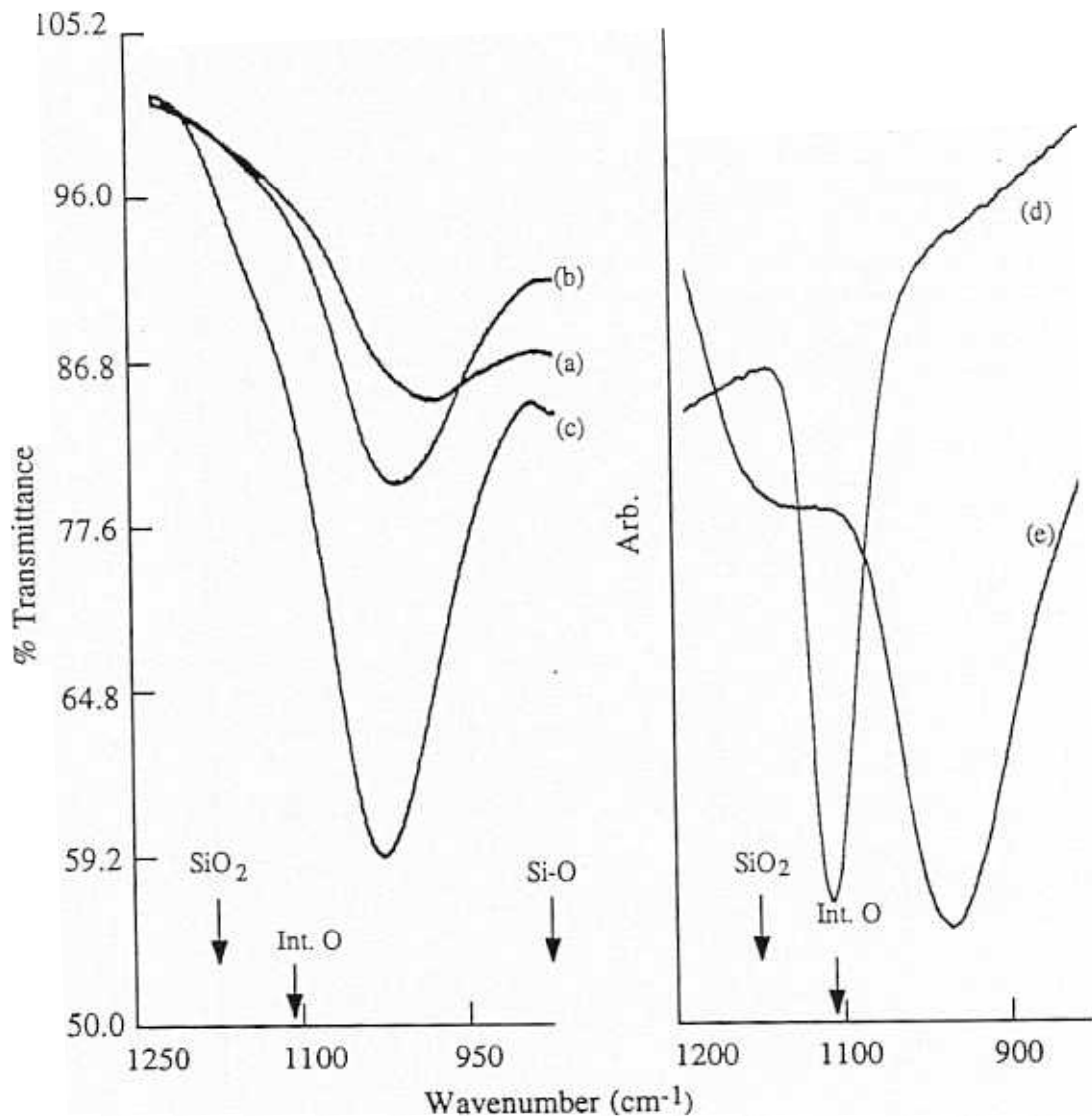
42

Figure 3.5. FTIR spectra of oxygen doped silicon. (a) is a film doped 5×10^{19} cm^{-3}, (b) 1×10^{20} cm^{-3}, and (c) 2×10^{20} cm^{-3} with oxygen. Films (a) through (c) were all grown at 750 °C using silane as the source gas. Plots (d) and (e) show purely interstitial oxygen in a bulk Cz wafer and an oxygen doped film with precipitate formation, respectively. Film (e) was grown at 850 °C using silane as the source gas. Notice that as the oxygen concentration increases from (a) to (c), the peak shifts toward higher energies and approaches the positioning of interstitial oxygen at 1107 cm^{-1}. The peaks of the oxygen doped layers are much broader suggesting a non-interstitial configuration for the oxygen.

43

We do not believe that SiO_2 precipitates are forming at the lower concentrations of oxygen (5×10^{19} to $\times 10^{20}$ cm^{-3}) because of the absence of the characteristic SiO_2 absorption line near 1200 cm^{-1} [25]. A shoulder near 1180 cm^{-1} in the FTIR spectrum becomes visible at a doping concentration of 2×10^{20} cm^{-3}. At extremely high concentrations of oxygen in the gas flow (200 ppm) and high growth temperatures (~ 850 °C), however, the IR spectrum becomes increasingly characteristic of SiO_2 with the primary absorption line moving closer to 1107 cm^{-1} and the shoulder near 1180 cm^{-1} and the films become visibly colorful and cloudy. The FTIR spectrum of such a film is shown in Figure 3.5 as well.

We used Secondary Ion Mass Spectrometry to calibrate the FTIR for the broadened and shifted absorption bands associated with the oxygen doped silicon. We found the conversion factor to be similar for unbroadened peak oxygen to within a factor of two.

We measured the oxygen concentrations in the silicon-germanium strained layers using SIMS. FTIR is not suited for measuring oxygen in germanium compounds for several reasons. First, the semiconductor standard for measuring oxygen in crystalline germanium has been discredited and consequently eliminated [26]. Second, to maintain a strained layer, film thicknesses of the silicon-germanium layer are kept below 1000Å. At this layer thickness, the cross section of Si-O and Ge-O bonds is too small to detect by FTIR even at concentrations of 10^{20} cm^{-3}. Figure 3.6 is a SIMS profile of a silicon-germanium layer grown at 625 °C sandwiched between two high temperature silicon layers. The oxygen concentration in this film reaches a level of approximately 10^{20} cm^{-3} and is characteristic of the early silicon-germanium heterojunction bipolar transistors which will be discussed in Chapter 5.

3.6 Oxygen Doping Kinetics and Crystallinity

Figure 3.7 plots the results of the oxygen doping experiments using the growth technique described in Section 3.4. For oxygen concentrations between 1 and 20 ppm in the total gas flow, we obtained oxygen concentrations in the range of 10^{20} cm^{-3} in the epitaxial films. Growth temperatures were 700 °C, 715 °C, 725 °C, and 750 °C, and the

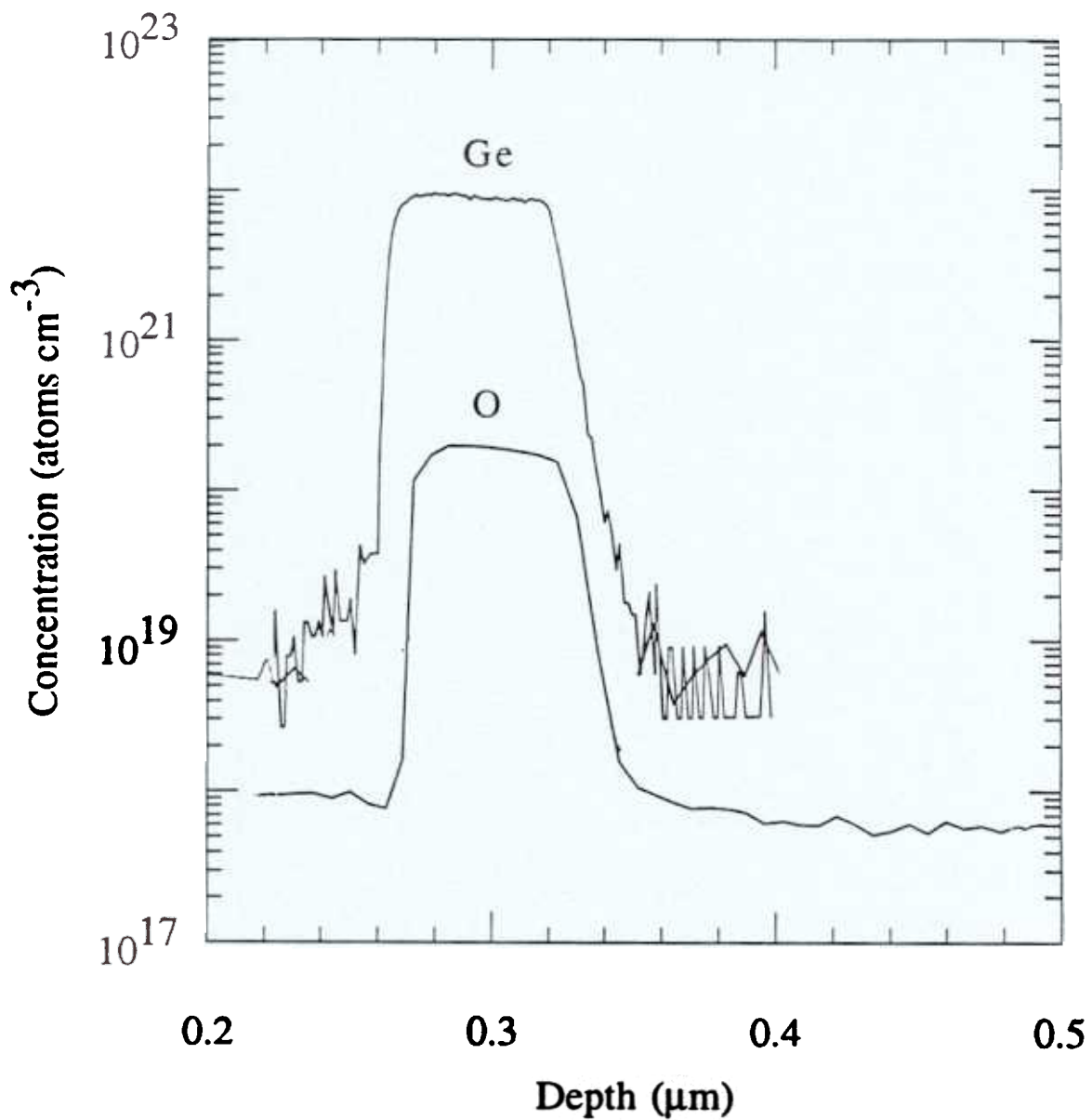Figure 3.6. SIMS plot of silicon-germanium contaminated with oxygen. The silicon-germanium is sandwiched between two layers of silicon grown at high temperature (>800 °C). The low temperature growth of silicon-germanium makes it more susceptable to oxygen contamination. This oxygen concentration was typical of the concentrations found in the base regions of the first HBT's grown in non-UHV systems.

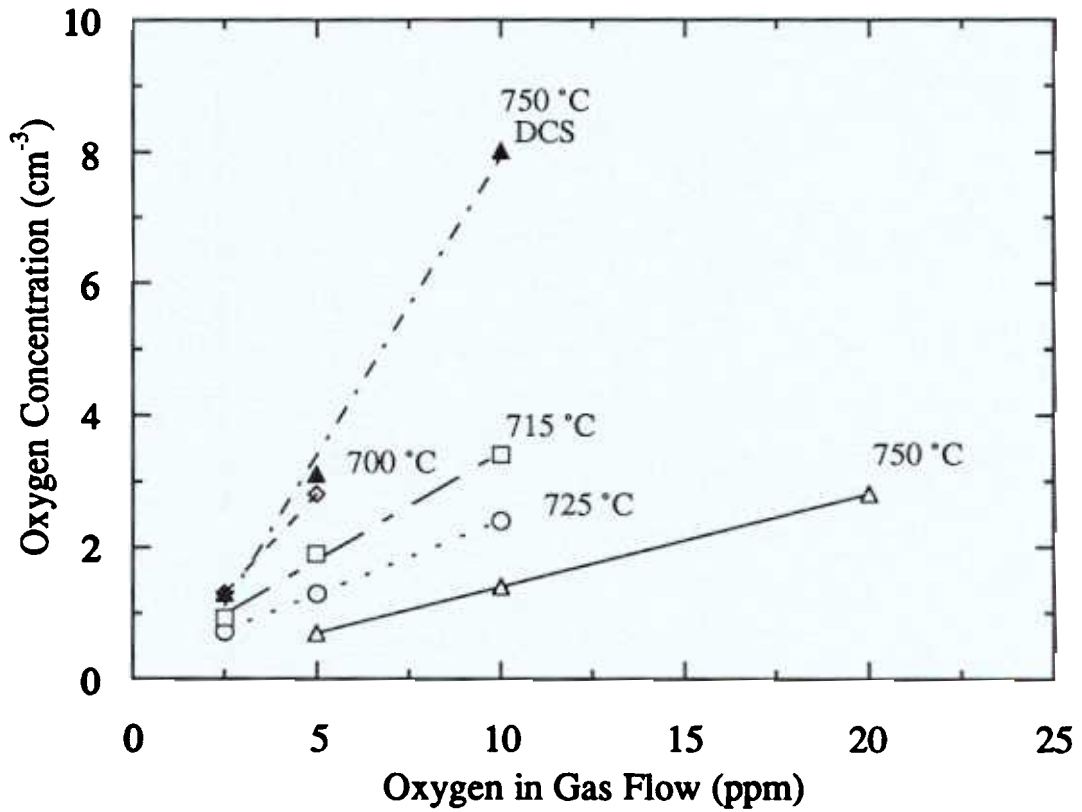45

Figure 3.7. Oxygen concentration in the silicon films as a function of oxygen concentration in the gas flow. The oxygen concentration in the gas flow is given in parts per million (ppm). There is a linear relationship between the oxygen concentration in the film and the oxygen partial pressure in the gas flow. The different lines correspond to the different growth temperatures of the layers.

corresponding growth rates were 133 Å/min, 183 Å/min, 235 Å/min and 485 Å/min, respectively. These oxygen concentrations are between one and two orders of magnitude above the peak solid solubility of oxygen in silicon ($\sim 10^{18}$ cm^{-3}), yet the layers remain crystalline. These oxygen concentration are still one or two orders of magnitude below the levels associated with semi-insulating poly-crystalline silicon (SIPOS) [24] and OXSEF [22]. Note that the oxygen concentration in the film is linear with the oxygen in the gas flow even in concentrations well above solid solubility. The concentration increases with decreasing temperature, but if we multiply by the growth rate and divide by the oxygen flow, we get the same oxygen sticking efficiency at all temperatures (see Figure 3.8). This indicates a strictly kinetic effect with no temperature dependence. Also shown in Fig. 3.7 is data for oxygen doping of silicon grown with DCS at 750 °C. The conditions were similar to those described in Sec. 3.4 except the source gas during the oxygen doping steps was DCS. The growth rate of this film is approximately 100 Å/min. (similar to SiH$_4$ at 700 °C) and the oxygen incorporation is similar to the oxygen doped SiH$_4$ growth. This indicates that the chlorine in the DCS does not have any significant effect on the oxygen incorporation.

We determined the crystallinity of the films using X-ray diffraction and electron channeling patterns (ECP). Figure 3.9 shows a diffraction pattern of a 3 μm thick silicon film doped to 5×10^{19} cm^{-3} grown with SiH$_4$ at 750 °C. The only peaks visible are those associated with crystalline silicon. If poly-silicon were present, a dominant peak at $\sim 28°$ would emerge due to the <111> plane of silicon as well as other peaks.

Electron channeling is a surface sensitive technique based on electron scattering from the silicon atoms within an elastic scattering length of the crystal surface (~ 10 Å). To conduct ECP, we grew crystalline silicon on top of the oxygen-doped silicon because the insulating nature of the oxygen-doped films prevents observation of ECP directly on the oxygen-doped layer. The ECP observed from the silicon cap layer are indistinguishable
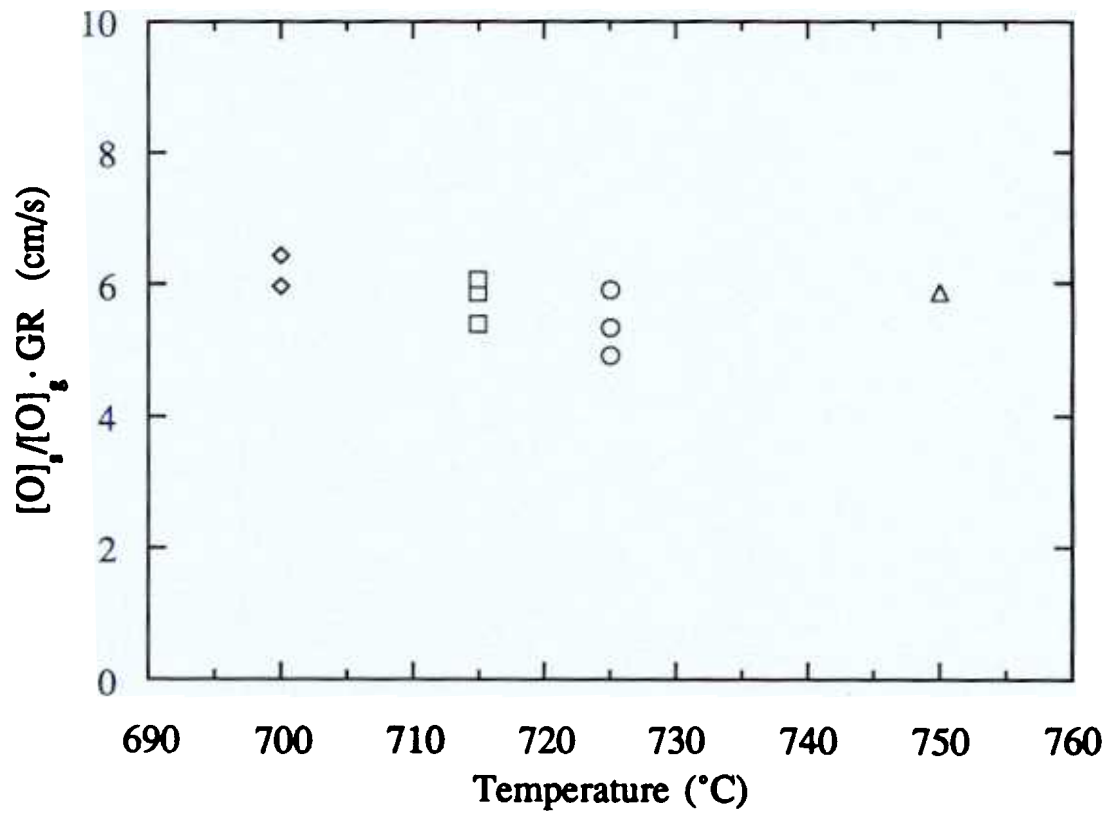
Figure 3.8. The normalized oxygen incorporation as a function of temperature. This is the data of Fig. 3.7 normalized by the growth rate and the oxygen flow. Notice that the incorporation rate is independent of temperature suggesting a kinetic limit to the oxygen incorporation.

48
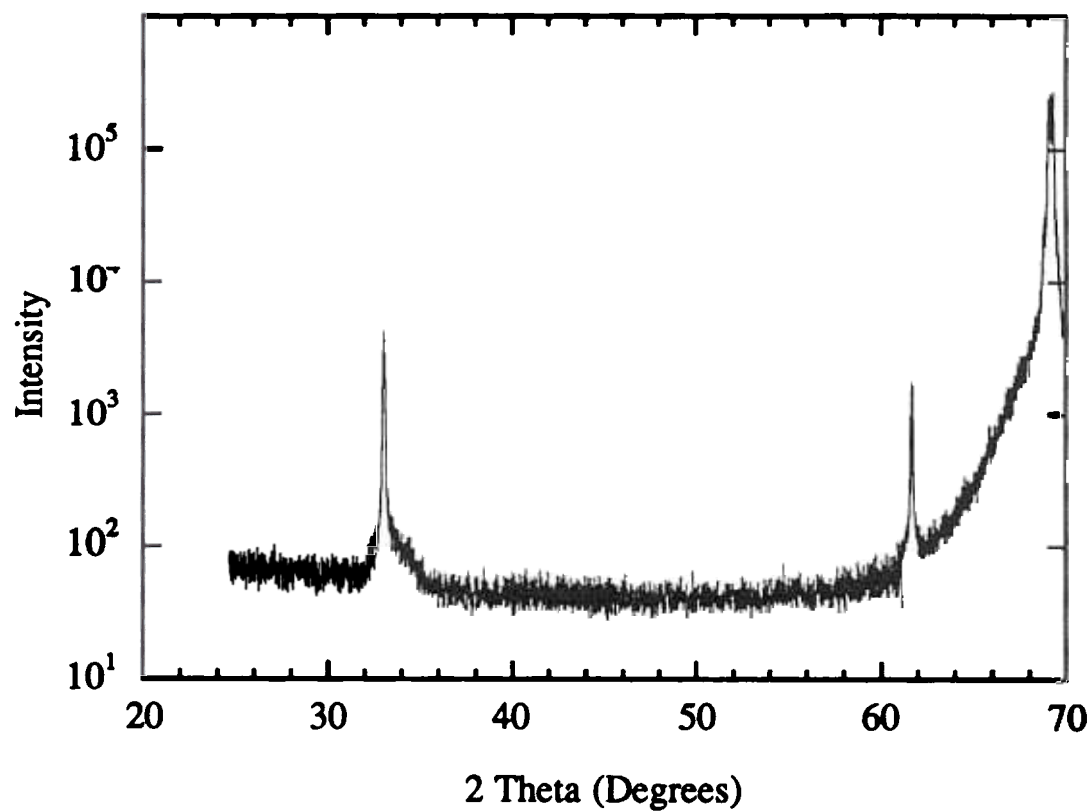
Figure 3.9. X-ray diffraction data for a 3 μm thick silicon film doped 5×10^{19} cm^{-3} with oxygen grown at 750 °C with silane. The only peaks present are those from crystalline silicon. The filter is not sufficient to block the ß line of the x-ray. If poly-silicon were present, a pronounced peak at $2\theta = 28°$ would appear in the spectrum.

from bulk silicon, demonstrating that the cap layer and the oxygen-doped films are crystalline. The implications of this will be discussed in Chapters 6 and 7.

In the next chapter, we will discuss the incorporation kinetics of oxygen during CVD growth. We will demonstrate that the effective sticking coefficient for oxygen on the silicon surface is greatly reduced from the UHV clean surface condition and use this information to determine the growth conditions for low-oxygen content films ($<10^{18}$ cm^{-3}).

3.7 References

1. N.C. Tung, "Application of Rapid Isothermal Annealing to Shallow P-N Junctions via BF_2 Implants," *J. Electrochem. Soc.* 132(4), 914 (1985).

2. J.F. Gibbons, C.M. Gronet and K.E. Williams, "Limited Reaction Processing: Silicon Epitaxy," *Appl. Phys. Lett.* (47)7, 721 (1985).

3. F.C. Eversteyn, "Chemical Reaction Engineering In The Semiconductor Industry," *Philips Res. Rept.* 19, 45 (1974).

4. P.M. Garone, P.V. Schwartz and J.C. Sturm, "Growth Rate and Doping Kinetics in Silicon-germanium Films Grown by Limited Reaction Processing," *Proc. Mater. Res. Soc.* 146, 341 (1989).

5. T.I. Kamins and D.J. Meyer, "Kinetics of Silicon-germanium Deposition by Atmospheric-pressure Chemical Vapor Deposition," *Appl. Phys. Lett.* 59(2), 178 (1991).

6. P.M. Garone, J.C. Sturm, P.V. Schwartz, S.A. Schwarz and B.A. Wilkens, "Silicon Vapor Phase Epitaxial Growth Catalysis by the Presence of Germane," *Appl. Phys. Lett.* 56(13), 1275 (1990).

7. R.E. Sheets, "Temperature Measurement and Control in a Rapid Thermal Processor," *Proc. Mater. Res. Soc.* 52, 191 (1986).

8. T. Sato, "Spectral Emissivity of Silicon," *Japn. J. Appl. Phys.* 6(3), 339 (1967).

9. Handbook of Optical Constants of Solids, E.D. Palik, ed., Academic Press, Orlando (1985).

10. J.C. Sturm, P.V. Schwartz and P.M. Garone, "Temperature Measurement by Infrared Transmission for Rapid Thermal Processing Applications," *Proc. Mater. Res. Soc.* 175, 401 (1990).

11. J.C. Sturm, P.V. Schwartz and P.M. Garone, "*In-situ* Temperature Measurement by Infrared Absorption for Low-temperature Epitaxial Growth of Homo- and Hetero-epitaxial Layers on Silicon," *J. Elect. Mat.* 19(10), 1051 (1990).

12   S.M. Sze, Physics of Semiconductor Devices, 2nd Ed., Wiley, New York, (1981).

13.   G.C. Macfarlane, T.P. McLean, J.E. Quarrington and V. Roberts, "Fine Structure in the Absorption-edge Spectrum of Ge," *Phys. Rev.* **108**(6), (1957).

14.   J.C. Sturm and C.M. Reaves, "Silicon Temperature Measurement by Infrared Absorption: Fundamental Processes and Doping Effects," *IEEE Trans. Elect. Dev.* **39**(1), 81 (1992).

15.   J.C. Sturm, P.M. Garone and P.V. Schwartz, "Temperature Control of Silicon-germanium Alloy Epitaxial Growth on Silicon Substrates by Infrared Transmission," *J. Appl. Phys.* **69**(1), 542 (1991).

16.   J.C. Sturm, P.V. Schwartz and P.M. Garone, "Silicon Temperature Measurement ny Infrared Transmission for Rapid Thermal Processing Applications," *Appl. Phys. Lett.* **56**(10), 961 (1990).

17.   D. Gräf, M. Grudner, R. Shultz and L. Mühlhoff, " Oxidation of HF-treated Si Wafer Surfaces in Air," *J. Appl. Phys.* **68**(10), 5155 (1990).

18.   C.W. Liu, J.C. Sturm, P.V. Schwartz and E.A. Fitzgerald, "Misfit Dislocation Nucleation Mechanisms and Metastability Enhancement of Selective $Si_{1-x}Ge_x$/Si Grown by Rapid Thermal Chemical Vapor Deposition," *Proc. Symp. Mat. Res. Soc.* **238** (1992).

19   Annual Book of ASTM Standards, "Standard Test Method for Interstitial Atomic Oxygen Content of Silicon by Infrared Absorption," **F 121-83**, (1983).

20.   W.A. Pliskin, "The Evaluation of Thin Film Insulators," *Thin Solid Films* **2**, 1 (1968).

21.   M. Tabe, M. Takahashi and Y. Sakakibara, "Oxygen-Doped Si Epitaxial Film (OXSEF)," *Japn. J. Appl. Phys.* **26**(11), 1830 (1987).

22.   T.J. Maloney, "MBE Growth and Characterization of Single Crystal Silicon Oxides on (111) and (100) Silicon," *J. Vac. Sci. Tech.* **B1**(3), 773 (1983).

23. W.R. Knolle, H.R. Maxwell, Jr., R.E. Beneson, "Hydrogen in Semi-insulating Polycrystalline Silicon Films," *J. Appl. Phys.* **51**(8), 4385 (1980).

24. T. Gong, *private communication concerning the Raman Spectrum of oxygen doped silicon.*

25. S.M. Hu, "Effects of Ambients on Oxygen Precipitation in Silicon," *Appl. Phys. Lett.* **36**(7), 561 (1980).

26. ASTM, *communication concerning the defunct standard* **F 122**.

Chapter 4

Incorporation Kinetics

4.1 Introduction

In this Chapter we discuss the kinetics of oxygen incorporation in silicon during low-temperature CVD growth. We describe the incorporation within the framework of the Grove model for CVD. We determine the effective sticking coefficient for oxygen on the surface of silicon under standard growth conditions and show that it is significantly reduced from the clean surface UHV condition of Chapter 2 due to the effect of hydrogen. With the effective sticking coefficient, we can then determine the conditions on gas purity for the low-temperature growth of low-oxygen content epitaxial silicon and silicon-germanium layers and then grow them in a non-UHV reactor.

4.2 Inadequacy of UHV Oxygen Sticking Models for CVD

In Sec. 3.6, we showed the oxygen incorporation rate to be strictly linear with gas flow and independent of growth rate, suggesting a simple kinetic model. At an oxygen concentration of 10 ppm, corresponding to a partial pressure of 60×10^{-6} Torr (assuming

a uniform distribution in the reaction chamber), the oxygen incorporation rate is 4.5 x 10^{11} atoms·cm^{-2}·s^{-1}. The oxygen incorporation given by:

$$O_{in} = 2 \cdot S \cdot [O]_{gas} \cdot v_{th} \qquad [4.1]$$

where O_{in} is the oxygen incorporation rate and $[O]_{gas}$ the concentration of oxygen in the gas flow, respectively, and S the probability of oxygen sticking to the silicon surface and v_{th} the thermal velocity of the oxygen molecules. If the sticking coefficient were 10^{-2}, as in the UHV condition, we expect oxygen incorporation rate of 3.2 x 10^{13} atoms·cm^{-2}·s^{-1}, approximately a factor of 100 higher than what we measure. This reduction of the incorporation rate is fortuitous for chemical vapor deposition. To explain this, we examine CVD kinetics and find that this is due to (1) hydrogen passivation of the surface and (2) the slow nature of the mass transport of oxygen across a boundary layer.

4.3 CVD Geometry

Gas flow and mass-transfer are complicated issues in CVD reactors. The simplest possible picture of mass-transfer is the stagnant film model depicted in Figure 4.1 [1]. In this picture we separate the gas phase into two regions, one which is well mixed and flows freely past the solid surface (free stream) and the other a stagnant layer (boundary layer) of thickness δ next to the substrate. The boundary layer exists because of the frictional drag on the gas as it passes the surface of the wafer. The transport of gas molecules across this boundary layer is by diffusion alone, with the following boundary conditions: (1) the gas concentration at the boundary-layer/free-stream edge is the free stream gas concentration (C_g); and (2) the concentration of gas at the substrate surface is C_s. The boundary layer is determined by the properties of the carrier gas and is the same for all species in the gas flow. The stagnant film model is then used to describe the conditions for mass transport during CVD growth.

4.4 Oxygen Incorporation

We describe the incorporation kinetics for oxygen using the Grove model for CVD[1]. For CVD, there are two key steps: 1) gases are transported to the substrate

Free Stream Gas Flow
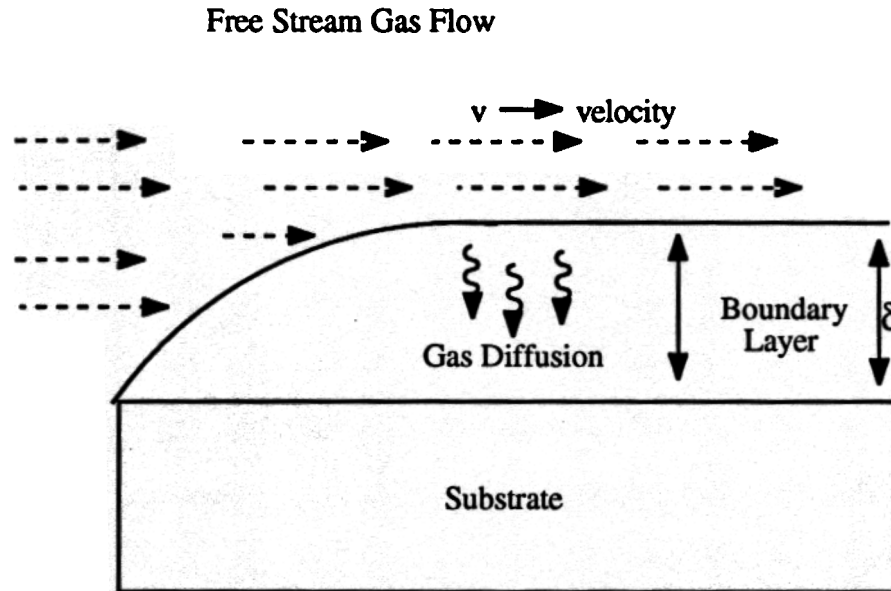
Figure 4.1. Boundary layer formation above the surface during CVD growth. The boundary layer forms above the substrate surface due to the frictional drag of the gases across the surface. Gas molecules must therefore diffuse from the free stream to the surface due to a concentration gradient. The concentration of the gas at boundary-layer/free-stream interface is C_g and at the substrate surface the gas concentration is C_s. $(C_s \leq C_g)$.

surface and 2) a chemical reaction occurs on the surface. Step 2) includes surface adsorption and all else that occurs on the wafer surface.

Transport of oxygen to the substrate surface across the boundary layer is governed by Fick's first law and is expressed as [1]:

$$F_d^{O_2} = h_g^{O_2} \cdot (C_g - C_s) \qquad [4.1]$$

where $F_d^{O_2}$ is the flux of oxygen atoms toward the substrate surface, $h_g^{O_2}$ is the mass transfer coefficient for oxygen ($= D_G/\delta$), and C_g and C_s are the concentrations of oxygen free stream and at the substrate surface (cm^{-3}). The surface reaction flux is assumed to be linearly proportional to the concentration of oxygen at the surface of the substrate and is mathematically represented as [1]:

$$F_s^{O_2} = k_s \cdot C_s \qquad [4.2]$$

where $F_s^{O_2}$ represents the flux of oxygen atoms consumed by the growing film and k_s is the surface reaction rate constant. In steady-state, these two fluxes, F_d and F_s, must be

By equating Eqns. 4.1 and 4.2 we obtain an expression for the surface concentration of oxygen, C_s:

$$C_s = \frac{h_g^{O_2}}{k_s + h_g^{O_2}} \cdot C_g \qquad [4.3]$$

Two limiting regimes can be seen from Eqn. 4.3: the mass-transport limited regime and the surface reaction limited regime. The mass-flow-limit occurs when the surface reaction rate is faster than the rate at which the gas molecules can reach the surface ($k_s \gg h_g$). Physically, this means that C_s approaches zero and is typical of high temperature growth because k_s is a strong function of temperature. At low temperatures, surface reactions limit the growth rate and k_s is significantly smaller than h_g. This situation is termed "reaction-rate-limited".

The flux of silicon atoms consumed at the surface is the product of the growth rate (G_{Si}) and the atomic density of atoms in the silicon crystal (5×10^{22} cm^{-3}). The silicon flux can be determined experimentally at any temperature. From the silicon flux and

Eqns. 4.2 and 4.3, we determine the density of oxygen atoms incorporating into the growing film as:

$$[O] = \frac{k_s \, h_g^{O_2}}{k_s + h_g^{O_2}} \cdot \frac{2 \, C_g}{G_{Si}} \qquad\qquad [4.4]$$

which is equivalent to taking the ratio of the oxygen and silicon fluxes consumed at the surface to be equal to the ratio of oxygen atoms to silicon atoms in the solid film. The factor of two in Eqn. 4.4 accounts for the two oxygen atoms in each oxygen molecule. Eqn. 4.4 is the starting point for determining the effective sticking coefficient for oxygen on the silicon surface during CVD growth.

4.5 Effective Sticking Coefficient

The effective sticking coefficient, or the probability that the oxygen atom at the silicon surface will stick to the silicon surface during CVD growth, is buried within k_s. By using Eqn. 4.4 and the data of Figure 3.7, the surface reaction rate constant can be extracted. The measurable quantities of Eqn. 4.4 are C_g, G_{Si} and $[O]$. We can determine the oxygen concentration in the gas flow from the flow rate into the reactor, and after growth, we can determine the growth rate of the layer by beveling and staining techniques. The oxygen concentrations in the films can be measured by SIMS and FTIR. The mass-transfer coefficient for oxygen does not depend upon the sticking probability and can be estimated from the growth rate of silicon in a mass-flow-limited growth regime.

The mass transfer coefficient, h_g, is defined as[1]:

$$h_g = D_G/\delta \qquad\qquad [4.5]$$

where D_G is the diffusivity of the gas and δ is the mean thickness of the boundary layer formed above the growth surface. D_G is inversely proportional to pressure (P^{-1}) and inversely proportional to the square root of temperature $(T^{-1/2})$ [2]. δ is independent of pressure and weakly dependent upon temperature $(T^{1/4})$. The boundary layer was discussed in Sec. 4.2. and is interpreted as a stagnant layer above the growth surface

where the gas stream does not move the molecules laterally along the growth surface. Rather, the gas molecules arrive at the growing surface by diffusion, due to a concentration gradient, across the boundary layer (see Figure 4.1). The steady-state boundary conditions require that the concentration of oxygen at the edge of the boundary layer equal the free stream oxygen concentration. The boundary layer is determined by the properties of the carrier gas (the carrier gas exceeds 99% of the total gas in the system) and is assumed to be the same for all gas species in the flow.

Direct calculation of h_g using Eqn. 4.5 is difficult because of uncertainties in the exact boundary layer thickness in a real reactor and because of the gradients in gas temperature from the wafer (700 °C to 1000 °C) to the reactor walls (estimated to be a few 100 °C). Rather the mass-transfer coefficient for oxygen can be estimated by measuring the mass-transfer coefficient for silicon in our growth reactor and correcting for the mass difference between O_2 and SiH_4 ($D_G \propto m^{1/2}$). Since the masses of O_2 and SiH_4 are equal (32 g/mole), however, the value obtained experimentally for h_g will be nearly equal for both molecules. The mass transfer coefficient for silane can be determined from the growth parameters for silicon. From a growth rate of 0.15 μm/min at 1000 °C for 0.5% silane in a hydrogen carrier at 6 Torr, we determine the flux of silane molecules toward the wafer surface in the mass flow limited regime ($C_S \approx 0$) as $h_g^{si}C_g =$ 1.2×10^{16} cm^{-2}s^{-1}. This is consistent, with an order of magnitude calculation of the flux ($D_G \cdot C_g/\delta = $ (80 cm^{2}s^{-} $\cdot 10^{15}$ cm^{-3}/ 4 cm) $= 2 \times 10^{16}$ cm^{-2}s^{-1}. The value of D_G is from Ref. [3] and δ is estimated from Eqn. 1.14 of Ref. [1]. Because the bulk of the gas in our reactor is hydrogen, h_g ($=D_G/\delta$) will not differ as the flow of gas under study (and hence C_g) is changed. Hence, C_g will scale linearly with the gas flow. Further, due to the similar masses of O_2 and SiH_4, at a given C_g, the product, $C_g h_g$, for O_2 and SiH_4 will be equal Finally, the $h_g C_g$ product is only weakly dependent upon temperature ($\sim T^{-1/4}$). Therefore using this value at other temperatures (e.g.. 700 °C) introduces little error. (The exact gas temperature is a complicated issue in cold wall reactors since a

temperature gradient is established between the wafer surface and the reactor walls.)
With the considerations given above, the measured value of $C_g h_g$ of 1.2×10^{16} cm^{-2}s^{-1} at
0.5 % O_2 in 6 Torr of H_2 will be used for our calculation (scaled to the appropriate O_2
gas flow).

We can re-configure Eqn. 4.4 to represent a measurable quantity to facilitate the
determination of the sticking probability. Rewriting Eqn. 4.4 as:

$$\frac{k_s}{k_s + h_g^{O_2}} = \frac{G_{Si}\,[O]}{2\,C_g^{O_2}\,h_g^{O_2}} \triangleq B \qquad\qquad [4.6]$$

gives us a ratio which can be determined experimentally. Table 4.1 lists the values of the
ratios for the data presented in Figure 3.7 for growth temperatures ranging from 700 °C to
750 °C. From the data in Table 4.1, it is apparent that we are in neither a mass flow
limited regime (B=0) nor a surface reaction limited regime (B=1).

To determine the surface sticking coefficient, we need k_s, the surface reaction rate
constant. To get k_s from Eqn. 4.6, we need C_g. Although we know the gas flow rates, it
is difficult to know C_g precisely because we know only the reactor pressure and wafer
temperature but not the gas temperature in the free stream. Therefore we assume (1) the
reactor walls are at 200 °C, (2) a linear temperature gradient is established between the
walls and the wafer and (3) the free stream is at the average temperature. With these
assumptions, we can get k_s from Eqn. 4.6. These values are in Table 4.1. We can now
determine the effective sticking coefficient from k_s.

It is known that the adsorption of oxygen to a clean silicon surface is not an
energy-activated process and depends on the probability of sticking with each collision
event [4]. The collision rate of oxygen on the surface of silicon is determined by the
thermal velocity of the oxygen molecules immediately above the wafer surface. The
surface reaction coefficient (as defined in Sec. 4.2) is therefore proportional to the
thermal velocity and a sticking probability:

Sample	Gas Source	T wafer (°C)	[O] (cm^{-3})	Growth rate (Å/min)	B	k_S (cm/s)	S_{eff}
676	DCS	750	3.1×10^{20}	100	0.21	6.7	2.4×10^{-4}
685	DCS	750	1.3×10^{20}	100	0.17	5.3	1.9×10^{-4}
826	SiH$_4$	750	1.4×10^{20}	485	0.22	7.3	2.7×10^{-4}
858	SiH$_4$	750	7.0×10^{19}	485	0.22	7.3	2.7×10^{-4}
855	SiH$_4$	725	1.2×10^{20}	235	0.20	6.5	2.3×10^{-4}
856	SiH$_4$	725	2.4×10^{20}	235	0.20	6.5	2.3×10^{-4}
967	SiH$_4$	700	2.8×10^{20}	133	0.24	8.2	2.9×10^{-4}
968	SiH$_4$	700	1.3×10^{20}	133	0.21	6.9	2.4×10^{-4}
969	SiH$_4$	715	9.1×10^{19}	183	0.22	7.3	2.7×10^{-4}
970	SiH$_4$	715	1.9×10^{20}	183	0.23	7.7	2.8×10^{-4}

Table 4.1. Data summarizing the incorporation kinetics of oxygen-doped silicon samples of Figure 3.7. [O] is the oxygen concentration incorporated into the growing film, B is the ratio of Eqn. 4.6, k_S is the surface reaction rate constant and S_{eff} is the effective sticking coefficient.